Spatial regulation of IRON MAN suppresses root iron acquisition upon microbial pattern perception

Min Cao[1], Matthieu Pierre Platre[1], Huei-Hsuan Tsai[2], Ling Zhang[1], Tatsuya Nobori[1,4], Laia Armengot[6,7], Yintong Chen[1], Wenrong He[1], Lukas Brent[1], Nuria Sanchez Coll[6,8], Joseph R. Ecker[1,4,5], Niko Geldner[2], and Wolfgang Busch[1,3,*]

[1] Plant Molecular and Cellular Biology Laboratory, Salk Institute for Biological Studies, La Jolla, California, USA
[2] Department of Plant Molecular Biology, University of Lausanne, Lausanne 1015, Switzerland
[3] Integrative Biology Laboratory, Salk Institute for Biological Studies, La Jolla, California, USA
[4] Genomic Analysis Laboratory, Salk Institute for Biological Studies, La Jolla, California, USA
[5] Howard Hughes Medical Institute, Salk Institute for Biological Studies, La Jolla, California, USA
[6] Centre for Research in Agricultural Genomics (CRAG), CSIC-IRTA-UAB-UB, Campus UAB, 08193 13 Bellaterra, Spain
[7] Department of Genetics, Microbiology and Statistics, Universitat de Barcelona, 08028 Barcelona, Spain
[8] Consejo Superior de Investigaciones Científicas (CSIC), 08001 Barcelona, Spain
[*] Correspondence: wbusch@salk.edu (W.B.)

Abstract

Iron is critical during host-microbe interactions. Restriction of available iron by the host during infection is an important defense strategy, described as nutritional immunity. However, this poses a conundrum for externally facing, absorptive tissues like the gut epithelium or the plant root epidermis that generate environments favoring iron bioavailability. For instance, plant roots acquire iron mostly from the soil and when iron deficient, increase iron availability through mechanisms that include rhizosphere acidification and secretion of iron chelators. Yet, the elevated iron bioavailability would also be beneficial for the growth of bacteria which threaten plant health. Here we report that microbial patterns such as flagellin lead to suppression of root iron acquisition via a localized degradation of the systemic iron deficiency signaling peptide IMA1. This response is also elicited when bacteria enter root tissues, but not when they dwell on the outer root surface. IMA1 itself has a role in modulating immunity in root and shoot, affecting the levels of root colonization and the resistance to foliar and vascular pathogens. Our findings uncover an adaptive molecular mechanism of nutritional immunity that affects iron bioavailability and uptake, as well as immune responses.

Iron is an essential nutrient for organismal growth throughout all branches of life [1,2]. Although iron is among the most common elements on our planet, its bioavailability in most environments is low and is a limiting factor for growth. Consequently, strong competition for iron is common between organisms. In mammals, iron levels have a direct impact on the composition of gut microbiota [3,4] and can modulate host inflammatory responses restricting iron availability for pathogenic microbes[5]. In plants, iron-limited soil environments trigger the activation of coumarin secretion in roots, which contributes to the alteration of the root-associated microbiota [6,7]. Conversely, the soil-borne *bacterial* community can also have a significant impact on root iron acquisition [6,8,9]. On the other side of the spectrum, pathogens can compete for and restrict iron for plants [10,11] , plant immunity responses affect bacterial iron homeostasis [12], and beneficial microbes can produce siderophores that pathogens cannot use, consequently suppressing pathogen growth [13,14]. Overall, iron plays an important but complex role in regulating plant-microbe interaction. However, much about this multifaced interaction that includes plants, beneficial or commensal and pathogenic microbes in the rhizosphere [15] remains to be learned.

Root iron deficiency responses are repressed by flg22

We had previously found a pronounced interplay of responses to low iron and immunity within the first few hours of roots exposed to an iron depletion environment [16]. To investigate this interplay at a longer timescale, we grew Arabidopsis seedlings in iron sufficient and low iron media with and without the elicitor flg22, a peptide fragment of bacterial flagellin (Fig.1a). Compared to seedlings grown under iron sufficient conditions (+Fe), seedlings grown on low iron conditions (-Fe) were slightly more chlorotic and contained less iron. This was drastically exacerbated when co-treated with flg22 (Fig.1a-c, Extended Data Fig.1a), but not when treated with a non-immunogenic form of flagellin, Flg20 (Extended Data Fig.1b-c). We therefore hypothesized that flg22 abolishes root iron uptake. To test this hypothesis, we measured ferric chelate reductase (FCR) activity and expression of the IRON REGULATED TRANSPORTER1 (IRT1), which are part of the canonical iron deficiency response in Arabidopsis and facilitate iron uptake. While FCR activity in roots was induced under -Fe without flg22 treatment, FCR activity was not induced in -Fe in the presence of flg22 (Fig.1d, Extended Data Fig. 1d). Likewise, lack of iron triggered the induction of the *pIRT1::NLS-2xYpet* marker[16] in the epidermal cells of the differentiation zone, and treatment with flg22, but not flg20, abolished

these responses (Fig.1e-f, Extended Data Fig. 1e). IRT1 protein levels reflected this response (Fig. 1g, Extended Data Fig. 1f-h). This was dependent on flg22 reception by the FLS2 immune receptor as flg22-induced chlorosis, and flg22-triggered FCR activity and IRT1 repression in -Fe conditions were abolished in *fls2* mutants (Extended Data Fig. 1i-m). Overall, these data demonstrated that flg22-elicited immune responses can repress the iron deficiency program.

The intriguing effect of flg22-triggered repression on iron deficiency responses prompted us to test other microbe-associated molecular patterns (MAMPs). The bacteria derived MAMP, elf18 triggers immune responses in the root tip as indicated by the upregulation of the reporters for several defense genes such as *FRK1*, *MYB51* and *CYP71A12* (Extended Data Fig. 2a-c). Like flg22, elf18 also repressed FCR activity and *IRT1* activation upon -Fe in differentiated epidermal cells (Extended Data Fig. 2d-f). Chitin, a fungal-derived MAMP triggered immuno-responses in the differentiation zone (Extended Data Fig. 2c), however, chitin treatment neither repressed FCR activity or *IRT1* activation in -Fe (Extended Data Fig. 2d-f). Taken together, our results suggest that different bacterial MAMPs modulate iron deficiency responses in the root in a specific manner.

IMA1 facilitates the crosstalk between flg22 and the iron deficiency response

The induction of FCR and IRT1 upon iron deficiency is controlled by the transcription factor FIT[17]. However, flg22 was still able to strongly repress IRT1 protein accumulation in plants that constitutively overexpress FIT (Extended Data Fig. 2g), suggesting that this response to flg22 might act more upstream in the iron deficiency pathway. To elucidate this, we conducted an RNAseq of roots grown under +/- Fe and/or +/- flg22. During the response to flg22, the expression of a large portion of iron responsive genes were modulated (Fig. 2a). The most significantly overlapping gene sets were constituted by genes that were downregulated in response to -Fe and upregulated in response to -Fe/+flg22 (hypergeometric test*; P*<$2.98*10^{-139}$), and vice versa (hypergeometric test*; P*<$2.08*10^{-92}$) (Extended Data Fig. 3a). K-means clustering of all differentially expressed genes (DEGs) that responded to either flg22, -Fe, or both (-Fe with flg22 double treatment) led to 5 clusters whose genes showed distinct expression patterns (Extended Data Fig. 3b). Cluster 5 was of most interest to us as it contained genes that were induced by -Fe, but strongly repressed by additional flg22 treatment. When conducting a gene ontology (GO) enrichment analysis for biological processes for the genes contained in cluster 5, we found that this gene list was highly enriched for the GO term “response to iron starvation”.

Among genes in cluster 5 were many of the canonical iron deficiency responsive genes, including those related to iron deficiency signaling (*BTS, PYE, bHLH38, bHLH39, bHLH100, bHLH101*), iron uptake-related components (*OPT3, NAS4, F6'H1, MYB10, IRT1, FRO2, MYB72, AHA7*) and mobile iron deficiency signaling (*IMA1*, *IMA2*, *IMA3*) (Fig. 2b). As expected, these responses were not observable in *fls2* mutant plants that don't perceive flg22 (Extended Data Fig. 3c-f). The extensive and distinct interplay of gene expression changes induced by flg22 and -Fe suggested that flg22 represses iron deficiency signaling by regulating key components of the iron deficiency signaling pathway.

Notably, flg22 repressed the upregulation of three IMAs in the root upon -Fe treatment (Fig. 2b). As IMAs act upstream of most known iron deficiency responses including FIT[18], we reasoned that IMAs might be downstream of the flg22 signaling relay. We therefore tested the overexpression line *IMA1ox* in which the iron deficiency pathway is constitutively activated in our conditions. Flg22-triggered leaf chlorosis and reduced iron concentration in the -Fe treated seedlings were largely restored in *IMA1ox* seedlings (Fig. 2c-e). Moreover, iron deficiency-induced IRT1 accumulation and FCR activation were insensitive to flg22 treatment in -Fe conditions in the *IMA1ox* line (Fig. 2f-g). An RNAseq experiment using *UBQ10::mCitrine-IMA1* and WT showed that unlike in Col-0 where a large proportion of genes that were upregulated under -Fe conditions were downregulated under -Fe/+flg22 (227/457, 49.7%; *p*-value: $2.08*10^{-92}$, hypergeometric test), there was no significant overlap of such genes in *UBQ10::mCitrine-IMA1* (Extended Data Fig. 4a, lower panel, 50/457, 10.9%; *p*-value: 0.99, hypergeometric test). The -Fe induced genes in Col-0 were upregulated in *UBQ10::mCitrine-IMA1* under +Fe condition, and shows less sensitive to flg22 treatment (Extended Data Fig. 4b-d). Consistent with previous findings [19], expression levels of IMA2 and IMA3 were decreased in *UBQ10::mCitrine-IMA1*, compared to Col-0 throughout all treatment conditions, suggesting that there might be a gene dosage compensation mechanism within the IMA gene family (Fig. 2h). We also examined the expression levels of key flg22 dependent PTI components[20,21] and found that some of these were also affected by IMA1 overexpression (Extended Data Fig. 4e). Taken together, our data show that the repression of iron deficiency responses by flg22 is abolished when IMA1 is continuously expressed, that the flg22 modulation of iron deficiency responses involves a downregulation of IMAs, and that IMA1 signaling can perturb expression of PTI response genes.

IMA1 is depleted by flg22 in the ground tissue to repress iron deficiency responses

IMA1 is a phloem mobile signal that is triggered upon iron deficiency [18]. To investigate whether and how flg22 abolishes IMA function, we obtained the IMA octuple mutant *ima8x*, and the rescue line, *pIMA1::EYFP-IMA; ima8x* [18]. As expected, we observed that IRT1 was not induced in iron deficiency condition in the *ima8x* mutant line and that the IMA1 transgene successfully rescued IRT1 induction in *ima8x* (Extended Data Fig. 5a). As in wildtype, flg22 was able to repress IRT1 accumulation and FCR induction in *pIMA1::EYFP-IMA*;*ima8x* (Extended Data Fig. 5a-b). To our surprise, the highly increased EYFP-IMA1 protein levels that we observed upon -Fe treatment in whole root tissue, were only slightly reduced upon flg22 treatment (Fig. 3a). To investigate this partial depletion of IMA1 protein in higher detail, we pretreated *pIMA1::EYFP-IMA*;*ima8x* with -Fe to strongly elevate IMA1 protein levels, and only subsequently treated with flg22. Consistent with the previous experiment, flg22 treatment for 6 hours only partially depleted the -Fe treatment-induced IMA1 in the root (Fig. 3b). As iron deficiency responses can be highly localized, we conducted confocal microscopy of EYFP-IMA1 in the early differentiation zone of the root, which is the region of *IRT1* induction under iron deficient conditions. As expected, -Fe highly induced IMA1 protein in stele, as well as in the pericycle, endodermis and cortex tissues in the roots of these seedlings (Fig.3c-d). Concomitant treatment with -Fe and flg22 strongly reduced IMA1 protein accumulation in the endodermis and cortex and partially in the pericycle, but it did not strongly reduce IMA1 level in the vasculature (Fig.3c-d). To quantify this pattern, we measured the IMA1 signal diameter and IMA1 signal intensity profile compared to the width of the whole root (Fig. 3e, Extended Data Fig.5h). Under -Fe, the IMA signal spread throughout the whole width of the root. In +Fe or when treated with flg22 in -Fe, it was restricted around the vasculature (Fig. 3f, Extended Data Fig.4h). As expected, these responses were abolished in the *fls2* receptor mutant that doesn't perceive flg22 (Extended Data Fig. 5c-h). We then set out to understand the mechanism for this cell-type specific depletion of IMA1 upon flg22 treatment. To study a potential transcriptional regulation, we obtained *pIMA1::mCitrine-NLS-mCitrine* plants. The *IMA1* transcriptional activity was low under +Fe, and -Fe strongly induced IMA1 transcription in all cell layers (Extended Data Fig.6a-b). Strikingly, flg22 didn't repress the *IMA1* transcriptional activity in the ground tissue under -

Fe, but even enhanced it (Extended Data Fig.6a&c). This suggested that the depletion of IMA1 in the ground tissue was more likely to be regulated at the post-transcriptional level.

IMA1 had been shown to be a mobile signal[18], and intercellular molecular movement can be regulated in plants by flg22-dependent callose deposition at plasmodesmata[22]. To test whether this could explain the flg22 mediated repression of -Fe responses, we applied 2-deoxy-d-glucose (DDG), a well-characterized callose synthase inhibitor[23]. The repression of IMA1 in the ground tissue coincided with the flg22 elicited repression of IRT1 and FCR. We therefore reasoned that we could use *IRT1* expression as a read-out to study the mechanisms by which IMA1 was repressed upon flg22 treatment. We couldn't observe a rescue of the IRT1 protein level (Extended Data Fig. 6d). This suggested that flg22 mediated callose deposition may not play a role in regulating the iron deficiency responses.

We then ectopically expressed mCitrine-IMA1 in a cell type specific manner (Extended Data Fig. 6e) and measured the IRT1 induction under iron sufficient condition, as this allowed us to exclude the effect of endogenous IMA, which is only induced by iron deficiency. IRT1 was strongly induced in *pUBQ10::mCitrine-IMA1* (expressing all cell layers), and *pPGP4::mCitrine-IMA1* lines (preferentially expressing in the epidermis and partially in the cortex) (Fig.3g). This suggested that the presence of IMA1 in the epidermis/cortex is critical and sufficient to induce IRT1 in the root. IRT1 was not strongly induced in the *pLBD16::mCitrine-IMA1* (pericycle) or in *pELTP::mCitrine-IMA1* lines (endodermis) compared to Col-0 wildtype plants (Fig. 3g). Interestingly and unlike *pIMA1::EYFP-IMA1;ima8x*, the signal of *pELTP::mCitrine-IMA1* did not extend to the outer cell layers under both +Fe and -Fe conditions, suggesting that IMA1 needs to be locally expressed in the cortex and epidermis to induce IRT1 (Extended data Fig. 7a-c).

We then tested whether constitutive presence of IMA1 in the epidermis and cortex was sufficient to abolish the repression of iron deficiency responses by flg22. *pPGP4::mCitrine-IMA1* roots driving IMA1 continuously in the epidermis and cortex root tissues were insensitive to the flg22-mediated IRT1 repression under +Fe conditions (Fig. 3h). We noted however, that the IMA1 levels were sightly decreased upon flg22 treatment in -Fe in the *pPGP4::mCitrine-IMA1* lines, suggesting IMA1 protein was degraded in this condition (Extended Data Fig. 7d). Taken together, our data strongly suggested that flg22 treatment leads to the repression of *IRT1* and

FCR activation under iron deficiency through downregulation of IMA1 in the outer tissue layers (ground tissue).

Flg22-triggered IMA1 depletion in the ground tissue is dependent on *BTSL1* and *BTSL2*

We next investigated whether the partial degradation of IMA1 that we had observed in -Fe flg22 conditions, acted through the ubiquitin dependent protein degradation pathway. MG132, an inhibitor of 26S proteasome, strongly reduced the protein degradation of IMA1 under -Fe (Extended Data Fig. 8a). As a previous study had shown that BRUTUS (BTS), a regulator of iron homeostasis, ubiquitinates IMA1 to mediate IMA1 degradation to regulate iron homeostasis [24], we hypothesized that BTS is required to mediate flg22-triggered IMA1 degradation. However, even though *bts-1* roots showed induced IRT1 expression and FCR activity compared to Col-0 under +Fe and -Fe conditions, IRT1 expression and FCR activity, as well as IMA1 in the ground tissue were still repressed upon flg22 treatment in *bts-1* mutant plants (Extended Data Fig. 8b-d). This suggested that BTS is not required for the flg22 mediated IMA1 degradation and iron deficiency response repression. There are two *BTS* homologs in Arabidopsis (*BTSL1* and *BTSL2)* that are expressed in the root and function redundantly to regulate iron homeostasis [25]. To test whether BTSL1 and BTSL2 are involved in regulating flg22-mediated iron responses, we phenotyped the *btsl1,2* double mutant in response to -Fe and flg22. Compared to Col-0, the *btsl1,2* mutant plants developed less leaf chlorosis in response to flg22 under low iron conditions, suggesting that *btsl1,2* plants are less sensitive to the flg22-triggered repression of iron deficiency responses (Fig.4a-c). Consistent with the chlorosis phenotype, FCR activity and IRT1 protein accumulation were significantly less responsive to flg22 treatment in -Fe conditions in *btsl1,2* mutant plants compared Col-0 (Fig.4d-e). These data suggested that *BTSL1* and *BTSL2* are required for regulating flg22-mediated repression of iron deficiency responses.

Next, we analyzed the expression pattern of *BTSL1* and *BTSL2* using *pBTSL1-GFP* and *pBTSL2-GFP* transgenic plants [25]. We observed that the expression levels of *BTSL1* and *BTSL2* were induced by -Fe (Fig. 4f). *BTSL1* is mainly expressed in the epidermis in response to iron deficiency. flg22 strongly repressed *BTSL1* expression. *BTSL2 is* mainly expressed in the entire ground tissue in iron deficiency conditions and in contrast to *BTSL1*, flg22 treatment didn't strongly repress *BTSL2* expression (Fig. 4f). Since the spatial expression patterns of *BTSL1* and *BTSL2* coincided with the area in which IMA1 was repressed upon flg22 treatment, we

hypothesized that BTSL1 and BTSL2 are involved in the flg22-regulated IMA1 depletion in the ground tissue. IMA1 protein level was reduced upon flg22 treatment in *pIMA1::EYFP-IMA1;ima8x*, but not in *pIMA1::EYFP-IMA1;btsl1,2* (Extended Data Fig. 8e-f). Consistent with our hypothesis, the strong increase of IMA1 in the ground tissue upon iron deficiency was not abolished by flg22 treatment in *btsl1,2* (Fig. 4g-i, Extended Data Fig. 8g). Cycloheximide (CHX) treatment decreased IMA1 level under -Fe, particularly in the epidermis and cortex, similarly to the effect of flg22 indicating that IMA1 is degraded in low iron conditions. This reduction of IMA1 by either CHX or flg22 was restored in *btsl1,2* (Extended Data Fig. 8h-j) indicating that BTSL1,2 degrade IMA1 protein under these conditions.

Taken together, our data indicate the flg22-induced suppression of the iron deficiency response is mediated predominantly through a BTSL1/2-dependent IMA1 degradation in the ground tissue of the root in the differentiation zone (Extended Data Fig. 8k).

IMA1 plays a distinct role to mediate immune responses in root and shoot

The iron deficiency response and an effective immune response trigger antagonistic responses in the root. For instance, the iron deficiency response includes the acidification of the rhizosphere for promoting iron solubility [26]. However, the defense response leads to an alkalization of the root meristem, which further promotes immunity [27]. Our data suggested that IMA1 might be a central player at the interface of both pathways. While the role of IMA1 in iron deficiency signaling has been well characterized, a role of IMA1 in the regulation of immunity had not been described yet. We therefore first investigated if IMA1 played a role in regulating the rhizosphere acidification capacity. We found that under +Fe conditions, Col-0 and *ima8x* exhibited no acidified roots whereas *UBQ10::mCitrine-IMA1* displayed constitutive root acidification (Fig.5a-b). Iron deficiency triggered root acidification around the root tip in Col-0, but not in *ima8x.* flg22 treatment repressed root acidification in Col-0, but not in *UBQ10::mCitrine-IMA1* (Fig.5a-b). This suggested that IMA-dependent signaling is required for abolishing the root acidification that is triggered by flg22. Although *UBQ10::mCitrine-IMA1* plants showed slightly shorter roots when they were grown on iron sufficient medium compared to Col-0 and *ima8x*, they exhibited less sensitivity to flg22 mediated root growth inhibition, whereas *ima8x* exhibited enhanced flg22 mediated root growth inhibition (Fig. 5c,e). Moreover, the less sensitive response of *UBQ10::mCitrine-IMA1* was restored by adding pH buffer reagent MES (Fig.5d-e), suggesting

that IMA1 dependent rhizosphere acidification is required to mediate root growth response to flg22. As FLS2 activity is dependent on environmental conditions, such as root apoplastic pH [28], we assessed if IMA1 affected FLS2 signaling through regulating rhizosphere pH. Consistent with the idea that IMA1-mediated root acidification might impair responses to flg22, roots of *UBQ10::mCitrine-IMA1* plants showed less MAPK phosphorylation upon flg22 treatment compared to Col-0 under iron sufficient conditions (Fig. 5f). We next checked another flg22 response gene, *CYP71A12* for which it had been shown that low pH dampens its promoter activation [28]. In line with this, qPCR experiments showed that *CYP71A12* induction by flg22 is impaired in *UBQ10::mCitrine-IMA1* plants, but is stronger in *ima8x* compared to Col-0 (Fig. 5g).

Iron availability has been shown to mediate root colonization by rhizobacterium *Bacillus velezensis* SQR9[29]. As our data suggested that IMA1 might be a central player in mediating iron and immune responses, we tested if IMA1 plays a role in mediating host-microbe interaction. The rhizobacterium *Pseudomonas protegens* CHA0 (a model commensal *Pseudomonas protegens* strain which produces flagellin) showed less colonization on the root of *ima8x*, whereas it colonized roots of the *UBQ10::mCitrine-IMA1* line to a higher extent (Fig. 5h). Taken together, this suggests that IMA1 functions at the nexus of iron deficiency and root-microbe interactions and that higher levels of IMA can facilitate elevated bacterial growth on roots.

Since IMA1 is considered a mobile signal that relays information from the shoot to the root [18], we checked if IMA1 also plays a role in coordinating iron and immune responses in the shoot. IMA1 protein level was low in the shoot under +Fe conditions. -Fe led to accumulation of IMA1 protein in the shoot in epidermal cells, mesophyll cells, and abundantly in in the vascular tissue (Extended Data Fig. 9a). Treatment with flg22 under -Fe conditions decreased IMA1 protein in the epidermal cells and mesophyll cells but not in the vascular tissue, suggesting that like in the root (Extended Data Fig. 9a), there are also cell-type specific regulatory mechanisms for IMA1 in the shoot. By analyzing *IMA1ox* dependent transcriptome changes in the shoot from a published dataset [18], we found that besides iron-responsive genes, innate immune response and systemic acquired resistance genes were enriched among the upregulated genes (Extended Data Fig. 9b). This suggests that IMA1 may also play a role in regulating immune programs in the shoot. However, we didn't observe any strong differences in flg22-elicited MAPK phosphorylation in the shoot when comparing *UBQ10::mCitrine-IMA1* and Col-0 wildtype

(Extended Data Fig. 9c), suggesting that the perception of flg22 or PTI signaling activation is not affected in *UBQ10::mCitrine-IMA1* in the shoot. To further explore this, we measured several PTI markers in shoot tissue using qPCR after plants had been exposed to flg22 for a short time (1 hour). Innate immunity marker genes were slightly upregulated without flg22, and the activation was more robust with flg22 in *UBQ10::mCitrine-IMA1* compared to Col-0. Moreover, ethylene and jasmonic acid biosynthesis and signaling pathways were not hyperactive in *UBQ10::mCitrine-IMA1*. This suggests that overexpression of IMA1 in the shoot induces a sub-set of systemic defense response, which is different from the root. We reasoned that plants might benefit from this induced systemic defense responses when they face pathogen attack. Consistent with this idea, *UBQ10::mCitrine-IMA1* plants were more resistance to foliar bacterial pathogen *Pseudomonas syringae pv. tomato* DC3000 (Extended Data Fig. 9e). Taken together, IMA1 plays an important role to coordinate iron deficiency and immunity, but the mechanism of action in roots and shoots may be different and might depend on the type of microorganism.

Iron deficiency responses are distinctly modulated by surface dwelling or invading bacteria

Bacterial populations can positively or negatively impact plant fitness through interactions that relate to iron. For example, commensal bacterial strains can aid roots with iron acquisition [6,30], whereas pathogens are thought to be in competition for available iron [13]. Recently, a spatially defined gating mechanism for cell damage dependent immune receptor activation that contributed to the distinction of commensal/beneficial and pathogenic bacteria was discovered [31]. Our data had shown that iron uptake and defense programs are connected by an IMA related mechanism in a spatially restricted manner. Thus, we wanted to test whether the repression of the iron signaling by a bacterial MAMP is dependent on the location of the bacteria. For this, we inoculated roots with CHA0-*mcherry/gfp2* under -Fe. Unlike with the flg22 treatment, the *pIRT1* reporter as well as the IRT1 protein induction were not fully repressed by CHA0 colonization (Fig.6a-b, Extended Data Fig.10a), showing that root colonization by this commensal bacterial strain does not strongly repress iron deficiency responses. Moreover, CHA0 colonization did not repress, but it even enhanced IMA1 protein induction by -Fe, whereas flg22 partially repressed IMA1 protein induction (Fig. 6c, Extended Data Fig.10b). When CHA0 was colonizing solely the surface of the root, IMA1 remained present in the outer cell layer, whereas flg22 treatment confined IMA1 into the stele (Fig. 6e-f). This indicates that this commensal/beneficial bacterial

strain colonization on root surface does not necessarily repress iron deficiency responses and that the plant is still able to take up iron.

During our inoculations, we noticed that in some cases, the CHA0 (which is considered a non-pathogenic bacterial strain) entered the roots at lateral root primordia, a region where cracks can naturally occur. Consistent with previous findings[31], higher immune responses were detected when CHA0 colonized at lateral root primordia compared with growth on the surface of differentiation zone (Extended Data Fig. 10c-d). When looking at such cases systematically, we found that when CHA0 entered the primary root through the LRP, IMA1 accumulation in the primary root was strongly reduced (Fig. 6g-h). Altogether, our data suggest that locally gated MAMP responsiveness can lead to spatially confined IMA1 repression and thereby might contribute to allow roots to locally shut off iron deficiency responses when internally colonized or to continue with iron acquisition in the presence of non-invasive, surface-dwelling bacteria (Extended Data Fig. 10e).

Our results reveal that the extended presence of the flg22 MAMP can abolish major components of the iron deficiency response in *Arabidopsis thaliana*. This seems puzzling, as transporting bioavailable iron into the root and therefore sequestering it, could deplete a potential pathogen of iron. However, these responses are only mounted when bioavailable iron is scarce in the environment (otherwise the plant wouldn't be iron deficient), therefore continuing to make iron bioavailable by exuding iron binding compounds and protons might benefit pathogens too. Taken together, we propose that the antagonistic function between the IMA1 mediated iron deficiency response and the flg22-elicited defense response might be critical to avoid making iron bioavailable for potential pathogens and to avoid impairing plant defense responses. Our findings also indicate that the modulation of iron deficiency responses is not a constitutive response that is triggered merely by the presence of bacteria but one that is triggered according to the presence of cues indicative of threats (e.g. sustained presence of high levels of flg22 or tissue damage). This finely tuned modulation would appear to be important to maintain a healthy rhizosphere during iron limiting conditions, as acidic (reducing) conditions and coumarins generally promote iron solubility in the rhizosphere. Shutting iron acquisition down might constitute a way to avoid enabling harmful bacteria the easy access to iron, but at the same time limits available iron for the plant itself as well as beneficial bacteria. However, limiting iron

availability in the rhizosphere generally might contain the risk for promoting the virulence of bacteria found in the rhizosphere, if it resembles the situation in the mammalian gut, where metabolic cooperativity and iron levels have been shown to suppress virulence [32].

A close linkage of nutrient stress response and the plant immune system has been observed for plant responses to phosphate[33,34] and points towards a general and complex intertwinement of nutrient acquisition and plant immune responses. For the conduit between iron and the immune system, IMAs appear to be a key component mediating a set of complex and multifaceted functions. On one hand IMA local degradation allows for shutting down root acidification, thereby enabling root responses to flg22, such as growth arrest and full phosphorylation of MAPKs. Consistent with these data, lack of IMA led to less colonization of the root with a surface dwelling commensal bacteria strain. On the other hand, IMA1 overexpressing plants were more resistance to foliar and vascular bacterial pathogens. It will be interesting to explore in the future to which extent modulation of iron acquisition and storage affects microbiome composition and microbial virulence in roots and shoots of plants.

ACKNOWLEDGMENTS

We thank Dr. Janneke Balk (John Innes Centre) for providing genetic materials *btsl1,2 (btsl1-1 btsl2-2), pBTSL1::GFP and pBTSL2::GFP* and Dr. Wolfgang Schmidt (Institute of Plant and Microbial Biology, Academia Sinica) for providing genetic materials *ima8x, IMA1ox and pIMA1::EYFP-IMA1;ima8x*. We thank Dr. Christoph Keel (University of Lausanne) for providing bacteria materials CHA0-*gfp2* and CHA0-*mcherry*. We thank the Salk Peptide Synthesis Core for synthesizing flg22 and flg20 peptides and the Salk Next Generation Sequencing Core Facility for NGS library preparation & sequencing. We also thank Sanghwa Lee, Charlotte Miller, Nicole Gibbs for critical comments on the manuscript. This study was funded by the National Institute of General Medical Sciences of the National Institutes of Health (grant number R01GM127759 to W. Busch), start-up funds from the Salk Institute for Biological Studies (W. Busch), funds from the Hess Chair in Plant Science (W. Busch), funds from the Taiwan's Ministry of Science and Technology (grant number 111-2917-I-564-021 to H. Tsai), funds from the Human Frontiers Science Program (HFSP) Long-term Fellowship (grant number LT000661/2020-L to T.Nobori), and it was supported by the NGS Core Facility of the Salk Institute with funding from NIH-NCI CCSG: P30 014195, the Chapman Foundation and the

Helmsley Charitable Trust. J.R.Ecker is an Investigator of the Howard Hughes Medical Institute. L.Armengot is supported by a Maria Zambrano postdoctoral fellowship by de Ministerio de Universidades and the European Union - NextGenerationEU. Research at CRAG was supported by grant MCIN/AEI/PID2019-108595RB-I00 funded by MCIN/AEI/10.13039/501100011033, grant TED2021-131457B-I00 funded by MCIN/AEI/ 10.13039/501100011033 and by the "European Union NextGenerationEU/PRTR", through the "Severo Ochoa Programme for Centres of Excellence in R&D" (CEX2019-000917 funded by MCIN/AEI/ 10.13039/501100011033), and by the CERCA Pro-gram/Generalitat de Catalunya (N.S.Coll).

AUTHOR CONTRIBUTIONS

M.C and W.B conceived the project and designed the experiments. M.C conducted most of the experiments. M.P.P assisted with confocal microscopy and conducted IMA1 imaging quantification. H.T provide protocol and conducted the bacteria inoculation experiment. L.Z performed RNAseq analysis. T.N. conducted *Pseudomonas syringae* pv. *tomato* DC3000 infection assay. L.A. conducted Ralstonia *solanacearum* infection assay for revision. Y.C conducted IMA1 imaging experiment in the shoot. W.H draw the schematic models for the manuscript. L.B assisted with generation of transgenic plants. W.B. , N.G. , J.E.R. , and N.S.C supervised work and provided funds and resources. M.C and W.B. wrote and revised the manuscript with input from M.P.P, H.T, Y.C.

DECLARATION OF INTERESTS

The authors declare no competing interests.

Materials and methods

Data and code availability

Raw sequencing data of RNAseq have been uploaded to NCBI GEO database: GSE213557. Scripts for imaging quantification and RNAseq analysis are available at https://github.com/cm010713/immunity-iron-project

Plant material and plant growth conditions

For all experiments, *Arabidopsis thaliana* ecotype Columbia (Col-0) was used as wild-type control. Plant seeds were sterilized in 70% ethanol for 8 minutes and washed with sterilized MilliQ water. Seeds were sowed on agar medium and stratified at 4 °C for 3 days in the dark. Seedlings were grown in Percival growth chamber (GENEVA SCIENTIFIC) at 22 °C and 16 hours light, 8 hours dark cycle. Iron sufficient (+Fe) medium was prepared according to the recipe of standard media as previously described[35]. The Gruber et al. medium contains: 750 µM of MgSO4−7H2O, 625 µM of KH2PO4, 1000 µM of NH4NO3, 9400 µM of KNO3, 1500 µM of CaCl2−2H2O, 0.055 µM of CoCl2−6H2O, 0.053 µM of CuCl2−2H2O, 50 µM of H3BO3, 2.5 µM of KI, 50 µM of MnCl2−4H2O, 0.52 µM of Na2MoO4−2H2O, 15 µM of ZnCl2, 75 µM of Na-Fe-EDTA (+Fe) or 10 µM of Na-Fe-EDTA (phenotype analysis), 1000 µM of MES adjusted to pH 5.5 with KOH, 0.5% Sucrose and 1% Difco Agar (BD, Cat# 214530, only for seedling growth on solid medium).

Generation of transgenic lines

To generate the different promoter driving IMA1 transgenic plants, the upstream promoter region based on the previous study[36] of *UBQ10* (AT4G05320, 1986 bp), *PGP4* (AT2G47000, 2174 bp), *ELTP* (At2g48140, 464 bp) and *LBD16* (AT2G42430, 2564 bp) was cloned into p5' (pDONR P4-P1r), the mCitrine CDS without stop codon was cloned into p221 (pDONR 221) and the IMA1 CDS with stop codon was cloned into p3' (pDONR P2r-P3) through BP reactions. The destination construct was combined using pB7m34GW, p221-mCitrine, p3'-IMA1 and one of the p5' vector using the multiple gateway LR reaction. The destination constructs were transformed into Col-0 and selected via Basta resistance to obtain homozygous T3 transgenic lines. To generate *pIMA1::mCitrine-NLS-mCitrine*, the same promoter region of *pIMA1::EYFP-*

IMA1;ima8x used the in previous study was cloned into p5' (pDONR P4-P1r) through BP reactions. The destination construct was combined using pB7m34GW, p221-mCitrine, p3'-NLS-mCitrine and p5'-IMA1pro using the multiple gateway LR reaction. The destination constructs were transformed into Col-0 and selected via Basta resistance to obtain homozygous T3 transgenic lines. To generate *pIMA1::EYFP-IMA1* in *bts-1*, *fls2* and *btsl1,2* mutant background, *pIMA1::EYFP-IMA1;ima8x* was crossed to *bts-1*, *fls2* and *btsl1,2* mutants, respectively, and the F3 homozygous transgenic plants were obtained for experimental analysis.

Elicitor preparation and treatment

Flg22 oligopeptide (QRLSTGSRINSAKDDAAGLQIA) and flg20 oligopeptide (QRLSTGSRINSAKDDAAGLQ) were synthesized by the Salk Peptide Synthesis Core. The elf18 oligopeptide (Ac-SKEKFERTKPHVNVGTIG) was obtained from EZbiolab. The peptides were dissolved in deionized water. Chitin (Frontier Scientific, Cat. JK399372) was dissolved in deionized water in 4°C with overnight rotating.

For elicitor treatment, flg22 and flg20 was added to the liquid medium to obtain the respective final concentration (depending on the time scale of the assay 2µM ,1µM, 100nM or 10nM as described in the figure legends). Chitin was diluted to 1mg/mL as the final concentration. Seedlings were treated in +Fe (75µM FeEDTA) or no Fe (0µM FeEDTA, 50µM FerroZine (ACROS Organics, Cat. 410570050)) liquid medium containing the elicitors for 24 hours, unless otherwise specified.

Protein extraction and western blot.

7-day-old seedlings grown on +Fe plates were transferred to liquid medium with +Fe (75µM Fe), +Fe+flg22 (75µM Fe + 100nM flg22), -Fe (50µM FerroZine), -Fe+flg22 (50µM FerroZine + 100nM flg22) and treated for 24 hours. For the protein extraction and western blot procedure, previously published method was used with minor modifications [37]. For IRT1, EYFP-IMA1 detection, 15 roots cut from the pretreated seedlings were harvested immediately in liquid nitrogen. The samples were ground with liquid nitrogen and lysed directly in 80µL total protein extraction buffer (50mM Tris-Cl pH 7.4, 150mM NaCl, 5mM EDTA, 1% SDS and 1% TritonX-100 supplemented with 1x NuPAGE™ LDS Sample Buffer (Invitrogen™, Cat. NP0008) and 1x NuPAGE™ Sample Reducing Agent (Invitrogen™, Cat. NP0009) for 15 minutes on ice. The

protein samples were denatured by heating for 10 minutes at 90°C and centrifuge at 13000rpm for 10 minutes. The supernatant protein samples were separated by NUPAGE 10% Bis-Tris Plus Gel (Invitrogen™, Cat.NW00105BOX) and transferred onto Nitrocellulose membrane by iBlot 2 Dry Blotting system (Invitrogen™, Cat. IB23001). IRT1 was detected by western blot with corresponding antibody (primary antibody, anti-IRT1 (Agrisera, Cat. No. AS111780) 1:2000 diluted in 5% non-fat milk; secondary antibody: Goat Anti-Rabbit IgG (H + L)-HRP Conjugate (Bio-Rad, Cat. No. 170-6515) 1:5000 in 5% non-fat milk). EYFP-IMA1, mCitrine-IMA1 and free GFP that expressed in CHA0 bacteria were detected by anti-GFP HRP conjugate antibody (Miltenyi Biotec, Cat. No. 130-091-833, 1:2000 diluted in 5% non-fat milk). FIT-3xHA was detected by anti-HA HRP conjugate antibody (Roche, Cat. No. 12013819001). The same membrane was stripped by the following steps (i) wash the membrane with 1M NaOH for 5 minutes, (ii) wash the membrane with 1x TBST, 5 minutes for 3 times. Then the membrane was re-blotted with Tubulin antibody as the internal control (Invitrogen™, Cat. 32-2500, 1:5000 in 5% non-fat milk; Goat Anti-Mouse IgG (H + L)-HRP Conjugate (Bio-Rad, Cat. No. 170-6516) in 5% non-fat milk).

Western blot for MAPK activity analysis

20 seedlings of 7-day-old light-grown Col-0 and *UBQ10::mCtritine-IMA1* on the +Fe plates without MES were treated in Fe sufficient liquid medium without MES with 1 μM flg22 peptide for 5 and 10 minutes. The root and shoot parts of the seedlings were harvested separately then the samples were ground with liquid nitrogen and lysed directly in 80μL (for root samples) or 150μL (for shoot samples) total protein extraction buffer (Same as described above). The phosphorylation status of MPK3,6 was detected by western blot with corresponding antibody (phospho-P44/42 MAPK antibodies (Cell Signaling, Cat. No. #4370) 1:2000 diluted in 1% BSA, Merck/Calbiochim, Cat. No.12657; Goat Anti-Rabbit IgG (H + L)-HRP Conjugate (Bio-Rad, Cat. No. 170-6515) 1:5000 in 5% non-fat milk). The same membrane was re-blotted with Tubulin antibody (root samples) (Invitrogen™, Cat. 32-2500, 1:5000 in 5% non-fat milk; Goat Anti-Mouse IgG (H + L)-HRP Conjugate (Bio-Rad, Cat. No. 170-6516) in 5% non-fat milk as an internal control.

Ferric chelate reductase activity measurement

7-day-old seedlings grown on +Fe plates were transferred to liquid medium with +Fe (75μM Fe), +Fe+flg22 (75μM Fe + 100nM flg22), -Fe (50μM FerroZine), or -Fe+flg22 (50μM FerroZine + 100nM flg22) and treated for 2 days. The seedlings were washed with deionized water for 5 times to remove any residual chemicals and 8-10 seedlings were pooled as one sample. The seedlings were incubated in the assay solution containing 0.1mM Fe (III)-DETA and 0.3mM FerroZine in the dark for 1 hour. The ferric chelate reductase activity was measured by spectrophotometry (Beckman Coulter, DU 730) with the absorbance (562 nm) of the Fe (II)-Ferrozine complex. The results were calculated on a root fresh weight basis by the formula:

FCR Activity (mmol/(g.hour))=OD(562)/29800*V(ml)/Fw(g)/T(hour)*10^6

Total chlorophyll concentration measurement.

The total chlorophyll content measurement is based on spectrophotometric analysis. Briefly, four shoots of the plants were harvested and pooled as one sample. Any liquid was carefully removed from the sample before the fresh weight was measured. Chlorophyll was extracted with 80% acetone in TissueLyser until the pellet became white. The leaf extracts were measured by spectrophotometry (Beckman Coulter, DU 730, 1 cm width cuvettes) with the absorbance (663 nm and 647nm), respectively. The results were calculated on a root fresh weight basis by the formula:

Total chlorophyll (a+b) (μg/mL)=(7.15 *A663)+(18.71*A647)

Total chlorophyll concentration= (Total chlorophyll * extract volume (mL))/ Fw (g)

Iron concentration measurement.

The total iron content was measured by a spectrophotometric method that was described previously[38]. The seedlings were harvested and rinsed with de-ionized water for 5 times and dried in an oven at 65°C for two days. After measure the dry weight, the tissues were digested with 65% (v/v) HNO_3 at 95°C for 6 hours, followed by adding 30% (v/v) H_2O_2 at 56°C for 2 hours. The iron content was analyzed in the assay solution (1 mM bathophenanthroline disulfonate (BPDS), 0.6 M sodium acetate, and 0.48 M hydroxylamine hydrochloride). The $FeCl_3$ solution was used to prepare the standard curve. The resulting Fe^{2+}-BPDS3 complex was measured with absorbance (535nm) using a microplate reader. The iron content in each sample

was calculated by the absorbance values against the standard curve and normalized by the dry weight (Dw).

Confocal microscopy for *pIRT1::NLS-2xYPet* and *pIMA1::EYFP-IMA1* with PI staining.

Seedlings were precultured on +Fe (75µM Fe) solid media for 4 days. For the treatment, around 8-10 seedlings were transferred to 5mL of +Fe (75µM Fe), +Fe+flg22 (75µM Fe + 100nM flg22), -Fe (50µM FerroZine), and -Fe+flg22 (50µM FerroZine + 100nM flg22) liquid medium in a 6-well plate and treated for 24 hours. For PI staining, pre-treated seedlings were stained with PI solution (2µg/mL, dissolved in MilliQ water) for 5 minutes and rinsed in water. Imaging experiment was performed on a Zeiss LSM710 confocal microscope with C-Apochromat 40x/1.20 W Korr M27 water objective lens. Ypet was excited with a 488 nm laser and fluorescence emission was filtered by a 505/550 nm filter. The PI signal is excited with either 488 or 514nm laser and fluorescence emission was filtered by a 600/650 nm filter. For the quantification of the raw intensity of the Ypet signal, the process has been automatized using the Fiji® software Macro, MACRO_Min_pIRT1_LSM710_PI-staining

For EYFP-IMA1 imaging in the leaf, 4-day-old *pIMA1::EYFP-IMA1;ima8x* seedlings were incubated in 5mL of +Fe (75µM Fe) , +Fe+flg22 (75µM Fe + 100nM flg22), -Fe (50µM FerroZine), and -Fe+flg22 (50µM FerroZine + 100nM flg22) liquid medium in a 6-well plate for 24 hours. Before imaging, cotyledons were excised and mounted in water, abaxial side of epidermis, mesophyll and vasculature regions were imaged using C-Apochromat 40x/1.20 W Korr M27 water objective lens. The bright field was imaged at the same time as a control. YFP was excited with a 514 nm laser and fluorescence emission was filtered by a 520/570 nm filter.

Microscopy setup for EYFP-IMA1 quantification.

Imaging experiments except when indicated below, were performed with the following Zeiss LSM710 confocal microscope set up: inverted Zeiss microscope using a Plan-Apochromat 20x/0.8 M27 objective lens. YFP was excited with a 514 nm laser (60mW) and fluorescence emission was filtered by a 519/580 nm filter.

Calculation of the EYFP-IMA1 mean gray values.

Eight Z-stack images were acquired in bright field and YFP signal representing a root section between 35 and 45µm. The brightfield images were processed with a Z-projection using the standard deviation method. From these images, the root area was detected using the plugin "Wavelet a trou" (http://www.ens-lyon.fr/RDP/SiCE/METHODS.html)[39]. The YFP images were processed with a Z-projection using the sum method. On those images the root area previous determined was reported and the mean gray value measured in this area to obtain the Mean gray value of the YFP channel. The process has been automatized using the Fiji® software Macro, MACRO_Intensity_IMA1.

Calculation of the EYFP-IMA1 diameter.

Eight Z-stack images were acquired in bright field and YFP signal representing a section between 35 and 45µm. The brightfield images were processed with a Z-projection using standard deviation method. The YFP images were processed with a Z-projection using the sum method. On Fiji® software, the root width was calculated using the straight line and on the same zone the width of the YFP signal was determined. The ratio of the YFP width was divided by the root width and multiplied by 100 to obtain the percentage of YFP-IMA1 tissue lateral diffusion.

Rhizosphere acidification assay and pH quantification

Col-0, *ima8x* and *UBQ10::mCitrine-IMA1* seedlings were precultured on +Fe (75µM Fe) solid medium for 7 days. The seedlings were transferred to +Fe solid medium or no Fe (0µM Fe, 50 µM FerroZine) solid medium for 3 days before the pH assay was carried out. The seedlings were then placed on a 1% agar plate containing 0.05% (w/v) bromocresol purple (pH 6.5 adjusted with NaOH) for 24 hours before being photographed.

Quantification of rhizosphere pH was conducted with a photospectromeric assay that was published with some modification[40,41]. 7-day-old seedlings grown on +Fe plates without MES were transferred to liquid medium with +Fe (75µM Fe), +Fe+flg22 (75µM Fe + 100nM flg22), -Fe (50µM FerroZine), or -Fe+flg22 (50µM FerroZine + 100nM flg22) without MES and treated for 2 days. Then the seedlings were transferred to the same liquid media supplemented with pH indicator bromocresol purple (0.005%) for 1 day in 48-well plates. Proton extrusion capacity was analyzed by reading the absorption at 590 nm (A590) with an automated microplate reader.

CHA0 Bacteria strain growth condition and inoculation.

The GFP or mCherry-labeled *Pseudomonas protegen*s strain, CHA0-*gfp2* (CHA0::attTn*7*-*gfp2*; Gm^r) and CHA0-*mCherry* (CHA0::attTn*7*-*mCherry*; Gm^r) were used for the bacteria inoculation assay[31]. The CHA0-*gfp2* or CHA0-*mCherry* strain was cultured in liquid LB medium (Miller's LB Broth, Research products international, Cat. L24040) supplemented with 25 µg/ml gentamycin at 28°C overnight. Bacteria cells were harvested by centrifugation (1 minute, 5000 rpm) and resuspended in sterile MilliQ water for 5 times to prevent potential element contamination from the LB medium.

For the bacteria inoculation experiment, the 4-day-old seedlings (imaging for IMA1 in DZ) or 7 -day-old seedlings (imaging for IMA1 in LRP) were precultured on +Fe (75µM Fe) solid medium were treated with liquid medium. Around 8-10 seedlings were transferred to 5mL of (Gruber medium with 0.25% sucrose) +Fe (75µM Fe), +Fe+CHA0 (75µM Fe + CHA0-*gfp2 or* CHA0-*mCherry*), -Fe (100µM FerroZine), -Fe+CHA0 (100µM FerroZine + CHA0-*gfp2 or* CHA0-*mCherry*), and -Fe+flg22 (100µM FerroZine + 100nM flg22) liquid medium in a 6-well plate and treated for 24 hours. For the liquid treatment with CHA0, the bacterial suspension was added in the well to a final OD_{600} of 0.05.

The effect of iron for CHA0 colonization of *Arabidopsis* roots was performed according to the previous studies with some modification ([6,29,31]) Briefly, 7 days old seedlings of Col-0, *ima8x* and *UBQ10::mCitrine-IMA1* were transferred to 5mL of (Gruber medium without and MES sucrose) +Fe (50µM FeEDTA pH 5.5), -Fe (100µM FerroZine), non-available iron (nAvFe 50µM $FeCl_3$ with pH 7.0) liquid medium in a 6-well plate and treated for 24 hours with prewashed CHA0-*mcherry* at the final OD 0.02. After the treatment, the roots were gentally washed with sterilized de-ionized water to remove the non-attached bacteria and the root length was measured. The roots were harvested in 1mL extraction buffer (10 mM $MgCl_2$, 0.01% Silwet L-77) and homogenized using TissueLyser with stainless steel beads. The samples were undergo dilution series from 10^1 to 10^6, and then spread on LB agar plates supplemented with 30µg/mL gentamycin. The CFUs were counted after 30 hours incubation at 28°C. The calculated CFUs were normalized by the root length.

***Pseudomonas syringae* pv. *tomato* DC3000 infection assay**

Arabidopsis thaliana Col-0 and *UBQ10::mCitrine-IMA1* were grown in a chamber at 22°C with a 12-h light period and 60-70% relative humidity for 30-31 days in the soil. *Pseudomonas syringae* pv. *tomato* DC3000 was cultured in the King's B (KB) liquid medium with antibiotics (Rifampicin and Tetracyclin) at 28°C. Bacteria were harvested by centrifugation and resuspended in sterile water to an OD_{600} of 0.001 (approximately 5 x 10^6 colony forming unit (CFU) ml^{-1}). *A. thaliana* leaves (2-3 fully-expanded leaves per plant) were infiltrated with bacterial suspensions using a needleless syringe. Two days after bacterial infiltration, two leaf discs (0.13 cm^2) per leaf were homogenized in 200 µl of $MgSO_4$, and a dilution series was streaked on KB plates. The plates were incubated at 28ºC for approximately two days before CFUs were counted.

Quantitative RT-PCR

7-day-old seedlings grown on +Fe solid medium were transferred to 5mL +Fe, +Fe +flg22, -Fe, and -Fe +flg22 liquid medium in a 6-well plate and treated for 24 hours unless specified. The root total RNA was isolated from around 15 roots (as a pool for one biological replicate) by using Spectrum™ Plant Total RNA Kit (Sigma-Aldrich, Cat. STRN250). 500ng of total RNA was reverse transcribed to cDNA using Maxima™ H Minus cDNA Synthesis Master Mix with dsDNase (Thermo Fisher, Cat. M1682). qRT-PCR was performed with Bio-Rad CFX384 Real-Time System and Luna qPCR mix (New England Biolabs, M3003L) according to the manufacturer's instructions. All the primers used for qRT-PCR analysis are listed in Supplementary Table 1.

RNAseq and data analysis

For transcriptomic analysis, 7-day-old seedlings grown on +Fe medium plates were transferred to 5mL +Fe, +Fe +flg22, -Fe, and -Fe +flg22 liquid medium in a 6-well plate and treated for 24 hours. 20 roots were pooled harvested as one biological replicate, with a total of three independent replicates per condition in each genotype (total sample numbers=36). The root samples were ground in liquid nitrogen and the RNA was extracted with the Spectrum™ Plant Total RNA Kit (Sigma-Aldrich, Cat. STRN250). The RNA quality and quantity were determined using a 2100 Bioanalyzer tape station (Agilent Technologies) and Qubit Fluorometer (Invitrogen). The sequencing libraries were generated by the Salk Next Generation Sequencing

Core according to Illumina manufacturer's instructions. Sequencing was performed using the Illumina Nextseq2000 platform.

Read alignment and generation of counts

RNA-seq short reads were mapped to the TAIR 10 reference genome which were obtained from the Arabidopsis Information resource web site (http://www.arabidopsis.org) [42] using the Splice Transcripts Alignments to Reference (STAR) version 2.7.0a [43]. A STAR index was built using the following parameters before mapping:

```
$ STAR --runThreadN 4 \
--runMode genomeGenerate \
--genomeDir ara_star_index \
--genomeFastaFiles <TAIR10.fa>\
--sjdbGTFfile <TAIR10.gtf> \
--sjdbOverhang 99
```

Then, RNA-seq reads in the FASTQ files were aligned to TAIR 10 and raw count files were generated using the following STAR command:

```
$ STAR --genomeDir ara_star_index \
--runThreadN 8 \
--sjdbOverhang 99 \
--sjdbGTFfile <TAIR10.gtf> \
--outSAMtype BAM SortedByCoordinate \
--outFileNamePrefix /output/small_ \
--outReadsUnmapped Fastx \
--quantMode GeneCounts \
--readFilesIn <fastq>
```

A custom R script (min_R_codes_for_manuscript) was used to combine counts per gene from count data produced from STAR cross all samples.

Differential expression analysis

Normalization of the read counts and differential gene expression analysis were performed using the R package, *edgeR* (version 3.36.0) [44]. The *CPM* (counts per million) function from *edgeR* was used to normalize the counts and differentially expressed genes (DEGs) by comparing the +Fe and -Fe treatment without or with flg22 were identified using *glmLRT* function from *edgeR*.

A false discovery rate (FDR < 0.05) and logFC (> 0 or < 0) were used as the criterial values for identification of up-regulated and down-regulated DEGs.

The DEG analysis was conducted by comparing different combinations of iron and flg22 treatments in wild type using ANOVA with *Benjamini-Hochberg* -corrected (FDR < 0.05) plus maximal absolute value of log2-converted fold change between pairs of treatment conditions larger than 1. Differentially expressed genes were visualized and k-means clustering method was used to classify DEGs via the *ComplexHeatmap* [45] package in R. The cluster number (k=5) was determined by total within-cluster sum of squared error and Bayesian information criterion (BIC). The boxplots were used to display scaled expression of genes from each cluster.

Gene ontology enrichment analysis was conducted using online tools of GENEONTOLOGY website: http://geneontology.org/

Statistical analysis

Statistical significance of overlap between DEGs from was assessed by *hypergeometric* distribution test. *Hypergeometric* test function in R was used to calculate statistical significance:

$ phyper(q-1, m, n-m, k, lower.tail = FALSE, log.p = FALSE)

q = the number of genes in common between two sets

m = the number of genes in Set 1;

n = the total number of genes in RNA-Seq counts table (33,602)

k = the number of genes in Set 2

For the Box & whiskers plot, the upper and lower boundary show min to max. The horizontal line in the box represents the median value.

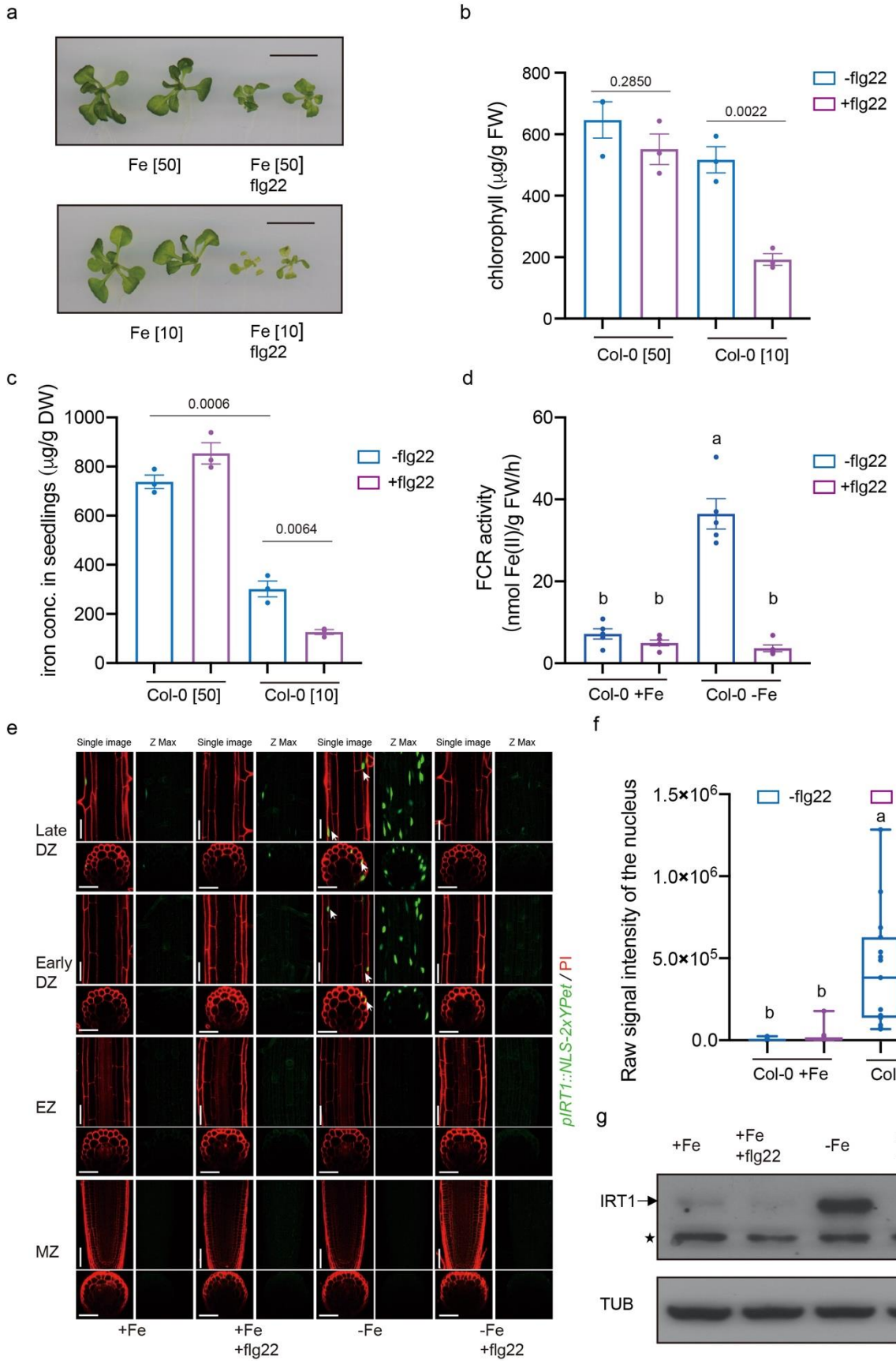
a
Fe [50]
Fe [50] flg22
Fe [10]
Fe [10] flg22
b
chlorophyll (µg/g FW)
0.2850
0.0022
-flg22
+flg22
Col-0 [50]
Col-0 [10]
c
iron conc. in seedlings (µg/g DW)
0.0006
0.0064
d
FCR activity (nmol Fe(II)/g FW/h)
Col-0 +Fe
Col-0 -Fe
e
Single image
Z Max
Late DZ
Early DZ
EZ
MZ
pIRT1::NLS-2xYPet / PI
+Fe
+Fe +flg22
-Fe
-Fe +flg22
f
Raw signal intensity of the nucleus
g
IRT1
TUB
kDa
30
25
50

Figure 1. flg22 represses iron uptake during iron deficiency.
(a-c) 15-day-old Arabidopsis seedling leaves in sufficient iron (50 µM) or low iron (10 µM) with or without low levels of flg22 (10 nM) treatment. (a) Shoots; Scale bar 1cm, (b) total chlorophyll concentration of Col-0 shoots, (c) Iron concentration of Col-0 seedlings; 3 biological replicates. Error bars: s.e.m.
(d) Ferric chelate reductase activity in Col-0 roots grown for 7 days under +Fe conditions and transferred to +Fe, +Fe with flg22, -Fe and -Fe with flg22 liquid media for 2 days. 5 biological replicates. Error bars: s.e.m. Different letters indicate statistically significant differences between different conditions analyzed by one-way ANOVA and Tukey's test ($p<0.05$).
(e) Promoter activity of *IRT1* in the root of *pIRT1::NLS-2xYpet* seedlings in response to +Fe, +Fe with flg22, -Fe and -Fe with flg22 treatment. seedlings were grown on the +Fe medium and after 5 days transferred to the different liquid media for 24 hours treatment. MZ: Meristematic zone; EZ: elongation zone; Green: Nuclear localized Ypet; Red: propidium iodide (PI) cell wall stain. For each treatment, a representative single confocal section (single image, GFP/PI), Maximum Intensity Z-Projection (Z-max, GFP only), a single optical section of the transverse view, and the Z-projection of the transverse section are shown. Scale bar, 50 µm.
(f) Raw signal intensity quantification of *pIRT1* reporter. $n\geq14$ biologically independent seedlings. Different letters indicate statistically significant differences between different conditions by one-way ANOVA and Tukey's test ($p<0.05$).
(g) Western blots showing IRT1 protein levels in Col-0 roots grown in +Fe, +Fe with flg22, -Fe and -Fe with flg22 treatment. Arrow indicates the IRT protein band. The asterisk indicates a non-specific band. Tubulin protein: internal control.

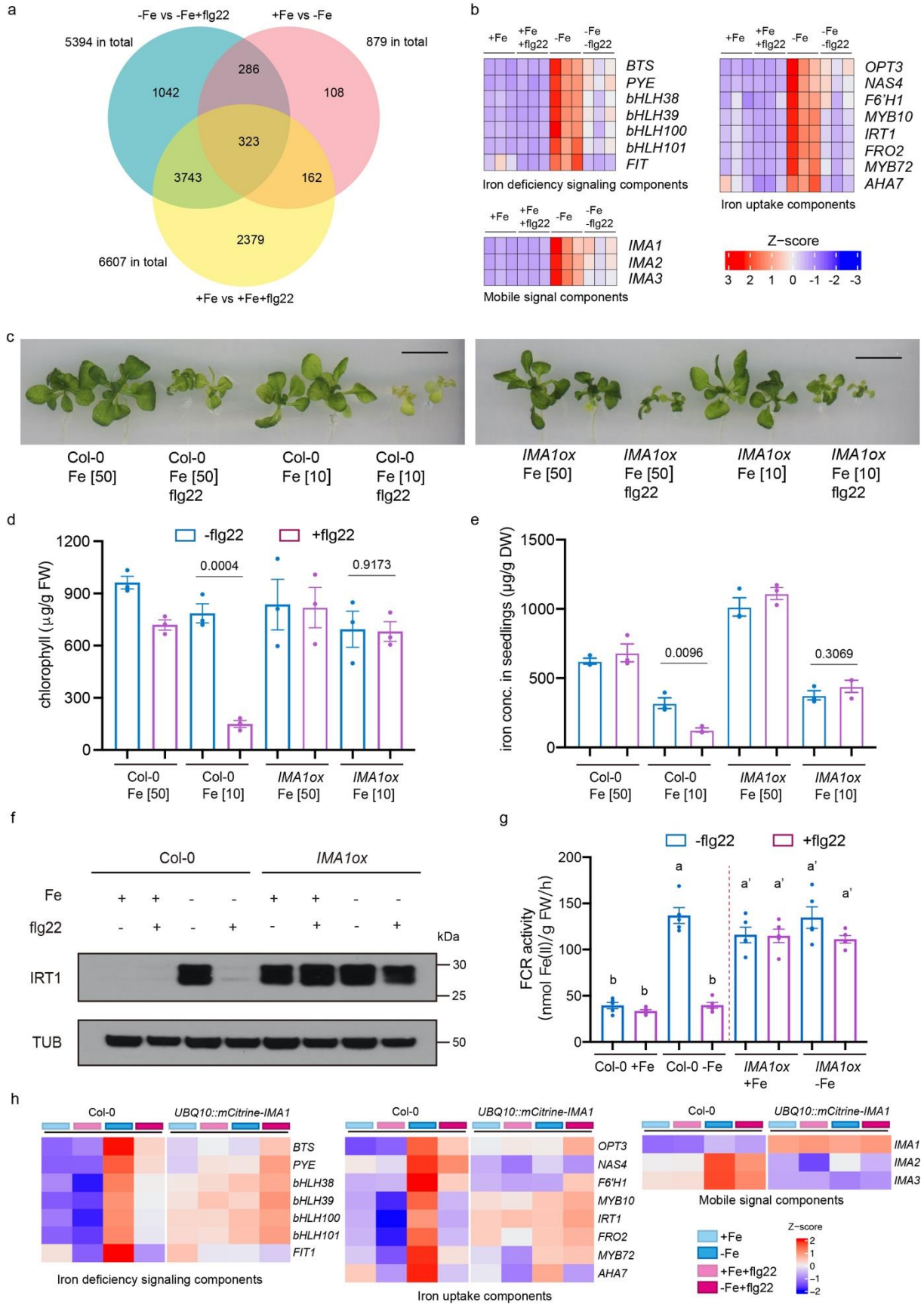
a
-Fe vs -Fe+flg22
+Fe vs -Fe
5394 in total
879 in total
286
1042
108
323
3743
162
2379
6607 in total
+Fe vs +Fe+flg22
b
+Fe
+Fe +flg22
-Fe
-Fe -flg22
BTS
PYE
bHLH38
bHLH39
bHLH100
bHLH101
FIT
Iron deficiency signaling components
OPT3
NAS4
F6'H1
MYB10
IRT1
FRO2
MYB72
AHA7
Iron uptake components
IMA1
IMA2
IMA3
Mobile signal components
Z-score
3 2 1 0 -1 -2 -3
c
Col-0 Fe [50]
Col-0 Fe [50] flg22
Col-0 Fe [10]
Col-0 Fe [10] flg22
IMA1ox Fe [50]
IMA1ox Fe [50] flg22
IMA1ox Fe [10]
IMA1ox Fe [10] flg22
d
-flg22
+flg22
chlorophyll (µg/g FW)
0.0004
0.9173
Col-0 Fe [50]
Col-0 Fe [10]
IMA1ox Fe [50]
IMA1ox Fe [10]
e
iron conc. in seedlings (µg/g DW)
0.0096
0.3069
f
Col-0
IMA1ox
Fe
flg22
kDa
IRT1
TUB
30
25
50
g
-flg22
+flg22
FCR activity (nmol Fe(II)/g FW/h)
Col-0 +Fe
Col-0 -Fe
IMA1ox +Fe
IMA1ox -Fe
h
Col-0
UBQ10::mCitrine-IMA1
BTS
PYE
bHLH38
bHLH39
bHLH100
bHLH101
FIT1
Iron deficiency signaling components
OPT3
NAS4
F6'H1
MYB10
IRT1
FRO2
MYB72
AHA7
Iron uptake components
IMA1
IMA2
IMA3
Mobile signal components
+Fe
-Fe
+Fe+flg22
-Fe+flg22
Z-score

Figure 2. flg22 represses iron deficiency responses through IMA1.
(a) Venn diagram of differentially expressed genes from RNAseq experiment.
(b) Heat map of mean-centered Z-scores for well-known iron responsive genes (3 independent biological repeats): iron deficiency signaling components, iron uptake components and long-distance signaling components.
(c-e) Phenotypes in 15-day-old Col-0 and *IMA1ox* seedlings in response to sufficient iron (50 µM) or low iron (10 µM) with or without low level flg22 (10 nM) treatment. (c) Shoots; Scale bar, 1cm. (d) Total chlorophyll concentrations of shoots. (e) Iron concentration of seedlings. (d,e) 3 biological replicates; Error bar: s.e.m. P-values from two-tailed Student t-test.
(f) Western blots showing IRT1 protein levels in Col-0 and *IMA1ox* roots is in response to +Fe, +Fe with flg22, -Fe and -Fe with flg22 treatment. Internal control Tubulin.
(g) Quantitative analysis of ferric chelate reductase activities in Col-0 and *IMA1ox* roots grown for 7 days under +Fe conditions and transferred to +Fe, +Fe with flg22, -Fe and -Fe with flg22 liquid media for 2 days. 5 biological replicates. Error bars: s.e.m. Different letters indicate statistically significant differences between different conditions analyzed by one-way ANOVA and Tukey's test ($p<0.05$).
(h) Heat map of mean-centered Z-scores (normalized to Col-0 +Fe) for well-known iron-responsive genes.

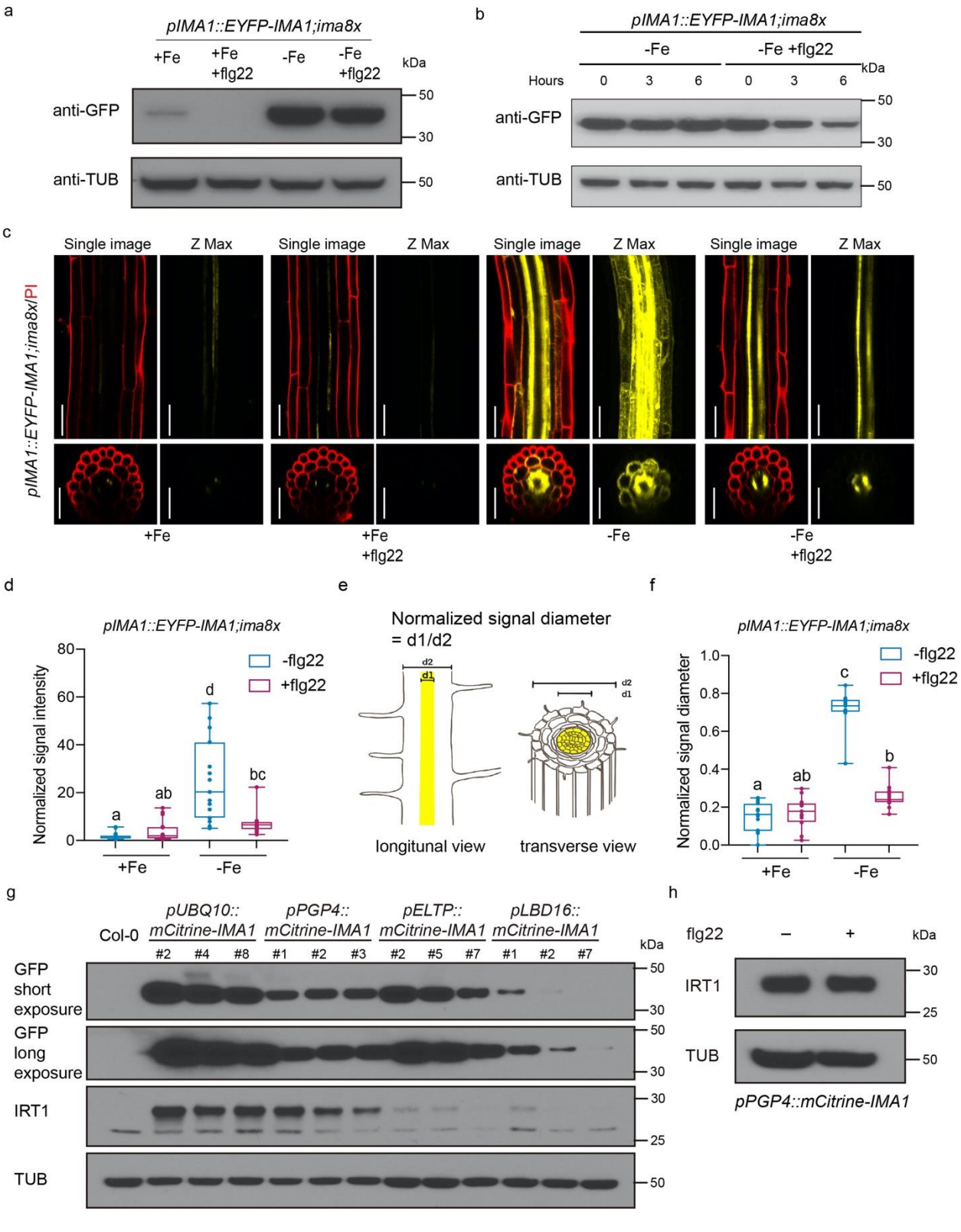
a
pIMA1::EYFP-IMA1;ima8x
+Fe
+Fe +flg22
-Fe
-Fe +flg22
kDa
anti-GFP
anti-TUB
50
30
50
b
pIMA1::EYFP-IMA1;ima8x
-Fe
-Fe +flg22
Hours
0 3 6 0 3 6
kDa
anti-GFP
anti-TUB
50
30
50
c
Single image
Z Max
pIMA1::EYFP-IMA1;ima8x/PI
+Fe
+Fe +flg22
-Fe
-Fe +flg22
d
pIMA1::EYFP-IMA1;ima8x
Normalized signal intensity
-flg22
+flg22
a
ab
d
bc
+Fe
-Fe
e
Normalized signal diameter
= d1/d2
d2
d1
longitunal view
transverse view
f
pIMA1::EYFP-IMA1;ima8x
Normalized signal diameter
-flg22
+flg22
a
ab
c
b
+Fe
-Fe
g
Col-0
pUBQ10:: mCitrine-IMA1
pPGP4:: mCitrine-IMA1
pELTP:: mCitrine-IMA1
pLBD16:: mCitrine-IMA1
#2 #4 #8 #1 #2 #3 #2 #5 #7 #1 #2 #7
kDa
GFP short exposure
GFP long exposure
IRT1
TUB
50
30
25
h
flg22
–
+
kDa
IRT1
TUB
30
25
50
pPGP4::mCitrine-IMA1

Figure 3. flg22 spatially represses IMA1 in the ground tissue of the root.
(a,b) IMA1 protein levels in *pIMA1::EYFP-IMA1;ima8x* roots. Internal control: Tubulin. (a) Response to +Fe, +Fe with flg22, -Fe and -Fe with flg22 treatment. (b) Time course: Seedlings were pre-treatment with -Fe for 36 hours, then treated with -Fe or -Fe+flg22 (1µm flg22) for 0, 3 and 6 hours.
(c) IMA1 distribution in response to +Fe, +Fe with flg22, -Fe and -Fe with flg22 treatment in differentiation zone of the root. Five-day-old *pIMA1::EYFP-IMA1;ima8x* seedlings were grown on +Fe medium and then transferred to liquid treatment medium for 24 hours. Yellow: EYFP-IMA1 signals; Red: Propidium iodide (PI) cell wall stain. For each treatment, a representative single confocal section (single image, EYFP/PI), a maximal Z-projection of the Z-stack (Z-max, EYFP only), a single optical section of the transverse view, and the Z-projection of the transverse section is shown. Scale bar, 50 µm.
(d) Quantification of IMA1 fluorescence signal intensity in the differentiation zone of roots (n=15 biologically independent seedlings). Different letters indicate statistically significant differences between different conditions analyzed by Multiple pairwise comparisons using the Steel-Dwass-Critchlow-Fligner procedure / Two-tailed test($p<0.05$).
(e) Schematic of quantification method for normalized signal diameter.
(f) Quantification of normalized IMA1 signal diameter in different treatment conditions in differentiation zones of the roots (n=15 biologically independent seedlings). Different letters indicate statistically significant differences between different conditions analyzed by Multiple pairwise comparisons using the Steel-Dwass-Critchlow-Fligner procedure / Two-tailed test($p<0.05$).
(g,h) Western blots showing IRT1 protein levels in roots of transgenic plant with different tissue-specific promoter driving IMA1 expression. Internal control Tubulin. (g) All seedlings were grown in +Fe to avoid the endogenous IRT1 induction by low iron. Three independent lines of each transgenic plants are shown (refer to extended data fig. 6e). (h) *pPGP4::mCtirine-IMA1* roots in response to +Fe and +Fe with flg22 treatment.

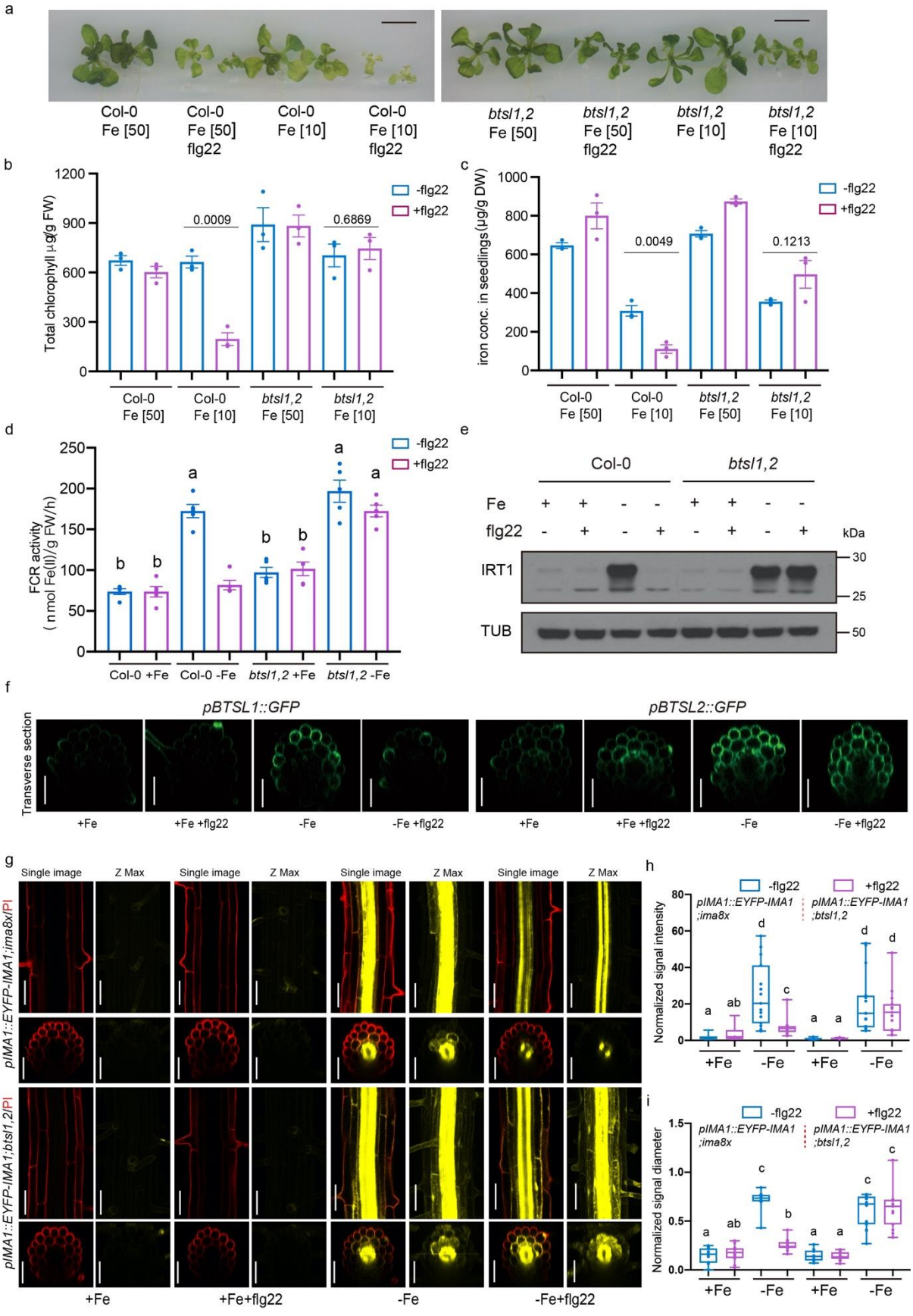
a
Col-0 Fe [50]
Col-0 Fe [50] flg22
Col-0 Fe [10]
Col-0 Fe [10] flg22
btsl1,2 Fe [50]
btsl1,2 Fe [50] flg22
btsl1,2 Fe [10]
btsl1,2 Fe [10] flg22
b
Total chlorophyll μg/g FW)
-flg22
+flg22
0.0009
0.6869
c
iron conc. in seedlings(μg/g DW)
0.0049
0.1213
d
FCR activity (n mol Fe(II)/g FW/h)
Col-0 +Fe
Col-0 -Fe
btsl1,2 +Fe
btsl1,2 -Fe
e
Col-0
btsl1,2
Fe
flg22
kDa
IRT1
TUB
30
25
50
f
pBTSL1::GFP
pBTSL2::GFP
Transverse section
+Fe
+Fe +flg22
-Fe
-Fe +flg22
g
Single image
Z Max
pIMA1::EYFP-IMA1;ima8x/PI
pIMA1::EYFP-IMA1;btsl1,2/PI
+Fe
+Fe+flg22
-Fe
-Fe+flg22
h
pIMA1::EYFP-IMA1 ;ima8x
pIMA1::EYFP-IMA1 ;btsl1,2
Normalized signal intensity
i
Normalized signal diameter

Figure 4. flg22 represses iron deficiency responses in the root via IMA1 degradation through BTSL1 and BTSL2.

(a-c) 15-day-old Col-0 and *IMA1ox* seedlings in sufficient iron (50 µM) or low iron (10 µM) with or without low level flg22 (10 nM) treatment. (a) Shoots; Scale bar, 1cm. (b) Total chlorophyll concentrations of shoots. (c) Iron concentration of seedlings. (b,c) 3 biological replicates; Error bar: s.e.m. P-values from two-tailed Student t-test.

(d) Ferric chelate reductase activities in Col-0 and *btsl1,2* roots grown for 7 days under +Fe conditions and transferred to +Fe, +Fe with flg22, -Fe and -Fe with flg22 liquid media for 2 days. 5 biological replicates. Error bar: s.e.m. Different letters indicate statistically significant differences between different conditions analyzed by one-way ANOVA and Tukey's test ($p<0.05$).

(e) Western blots showing IRT1 protein levels in Col-0 and *btsl1,2* roots in +Fe, +Fe with flg22, -Fe and -Fe with flg22 treatment. Internal control Tubulin.

(f) Transverse confocal microscopy sections of the of the differentiation zone of the root in *pBTSL1-GFP* and *pBSTL2-GFP* in response to +Fe, +Fe with flg22, -Fe and -Fe with flg22 treatments. Green: GFP channel; scale bar, 50 µm.

(g) Confocal microscopy images of IMA1 distribution in response to +Fe, +Fe with flg22, -Fe and -Fe with flg22 treatment in the differentiation zone of the root. 5-day-old *pIMA1::EYFP-IMA1;ima8x* and *pIMA1::EYFP-IMA1;btsl1,2* seedlings were grown on +Fe medium and then transferred to different liquid media for 24 hours treatment. Yellow: EYFP-IMA1; Red: Propidium iodide (PI) cell wall stain. For each treatment, a representative single confocal section (single image, EYFP/PI), a maximal Z-projection of the Z-stack (Z-max, EYFP only), a single optical section of the transverse view, and the Z-projection of the transverse section is shown. Scale bar, 50 µm.

(h-i) Quantification of IMA1 fluorescence signal intensity (h) and normalized IMA1 signal diameter (i) in response to +Fe, +Fe with flg22, -Fe and -Fe with flg22 treatment in differentiation zone of roots in *pIMA1::EYFP-IMA1;ima8x* and *pIMA1::EYFP-IMA1;btsl1,2* ($n\geq14$ biologically independent seedlings). The same dataset as shown in Fig.3 e&f of *pIMA1::EYFP-IMA1;ima8x* was used here as the images for quantification were taken at the same time under the same condition. Different letters indicate statistically significant differences between different conditions analyzed by Multiple pairwise comparisons using the Steel-Dwass-Critchlow-Fligner procedure / Two-tailed test ($p<0.05$).

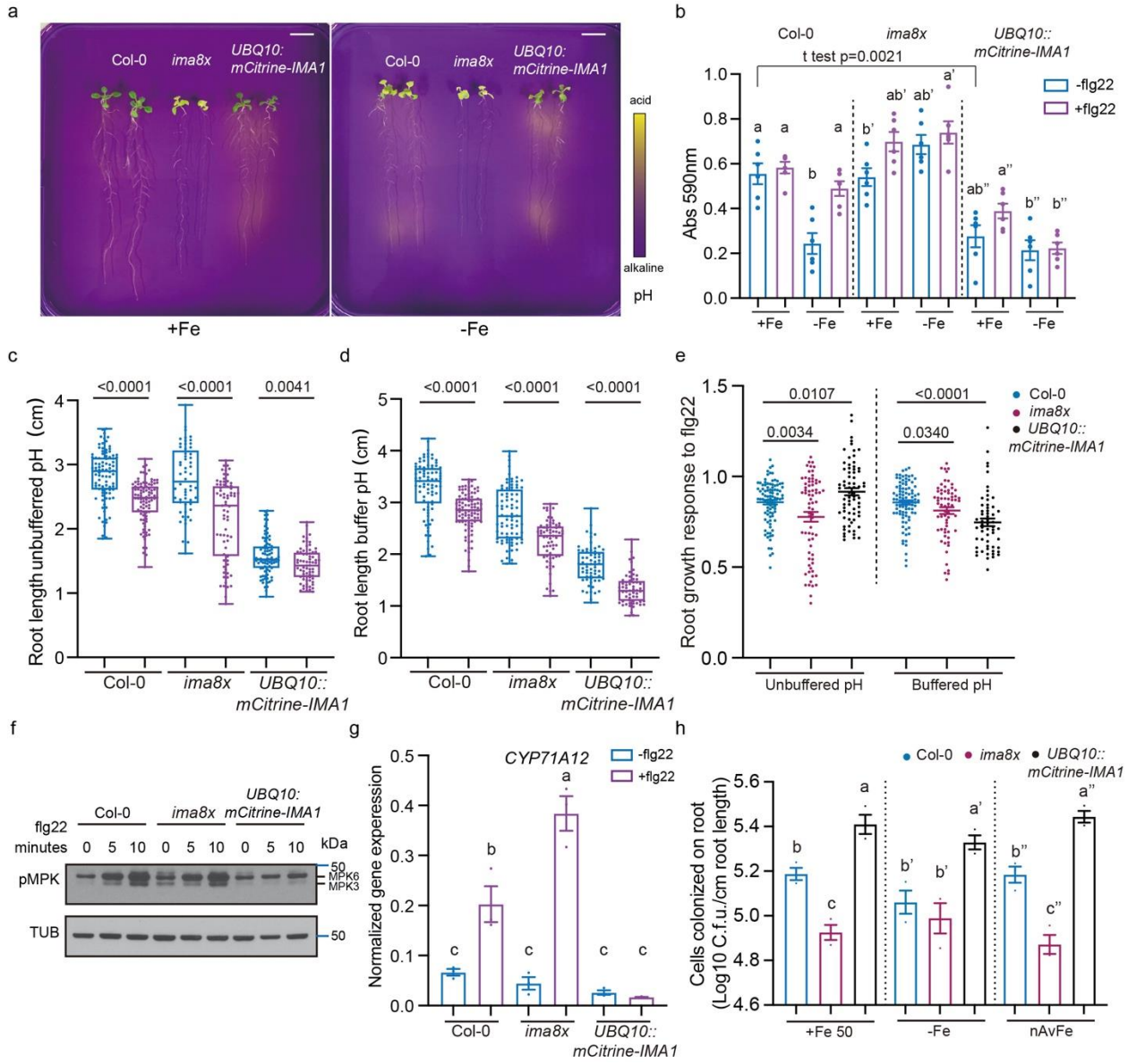
a
Col-0
ima8x
UBQ10:
mCitrine-IMA1
acid
alkaline
pH
+Fe
-Fe
b
t test p=0.0021
-flg22
+flg22
Abs 590nm
c
Root length unbuffered pH (cm)
d
Root length buffer pH (cm)
e
Root growth response to flg22
Unbuffered pH
Buffered pH
f
flg22
minutes
kDa
pMPK
MPK6
MPK3
TUB
g
CYP71A12
Normalized gene expression
h
Cells colonized on root
(Log10 C.f.u./cm root length)
+Fe 50
-Fe
nAvFe

Figure 5. IMA1 dependent rhizosphere acidification regulates immune-responses and bacterial colonization of the root.

(a,b) Rhizosphere acidification responses of Col-0, *ima8x* and *UBQ10::mCitrine-IMA1* in +Fe and -Fe treatment. Bromocresol purple was used as pH indicator. Yellow color indicates lower pH (acid).

(b) Standard media acidification by Col-0, *ima8x* and *UBQ10::mCitrine-IMA1* in response to +Fe, +Fe with flg22, -Fe and -Fe with flg22 treatments. 6 biological replicates. Error bar: s.e.m. Different letters indicate statistically significant differences between different conditions within each genotype analyzed by one-way ANOVA and Tukey's test ($p<0.05$). Two-tailed Student t-test shows statistically significant difference of media acidification of Col-0 and *UBQ10::mCitrine-IMA1* under +Fe.

(c,d) Quantification of root length of Col-0, *ima8x* and *UBQ10::mCitrine-IMA1* in +Fe and +Fe+flg22 conditions (c) without MES-KOH and (d) with 1mM MES-KOH. P-values from two-tailed Student t-test.

(e) Quantification of flg22-mediated root growth responses (+flg22/-flg22) of Col-0, *ima8x* and *UBQ10::mCitrine-IMA1* with/without MES-KOH. Horizontal line: mean; Error bars s.e.m. P-values from two-tailed Student t-test.

(f) Western blots showing MAPK phosphorylation by flg22 in Col-0, *ima8x* and *UBQ10::mCitrine-IMA1* roots in response to flg22. The roots were treated with 1µM flg22 for 0, 5 and 10 minutes. Internal control Tubulin.

(g) *CYP71A12* transcript level in +Fe and +Fe with flg22 by quantitative RT-PCR. Roots were treated with 1µM flg22 for 1 hour. Normalized to *ACT2*. 3 biological replicates. Error bars: s.e.m. Different letters indicate statistically significant differences between different conditions analyzed by one-way ANOVA and Tukey's test ($p<0.05$).

(h) Colonization of 7-day-old Arabidopsis roots at 1 d post-inoculation by CHA0 under +Fe, -Fe and non-available iron (nAvFe) conditions. 3 biological replicates. Error bars: s.e.m. Different letters indicate statistically significant differences between different genotypes analyzed by one-way ANOVA and Tukey's test ($p<0.05$).

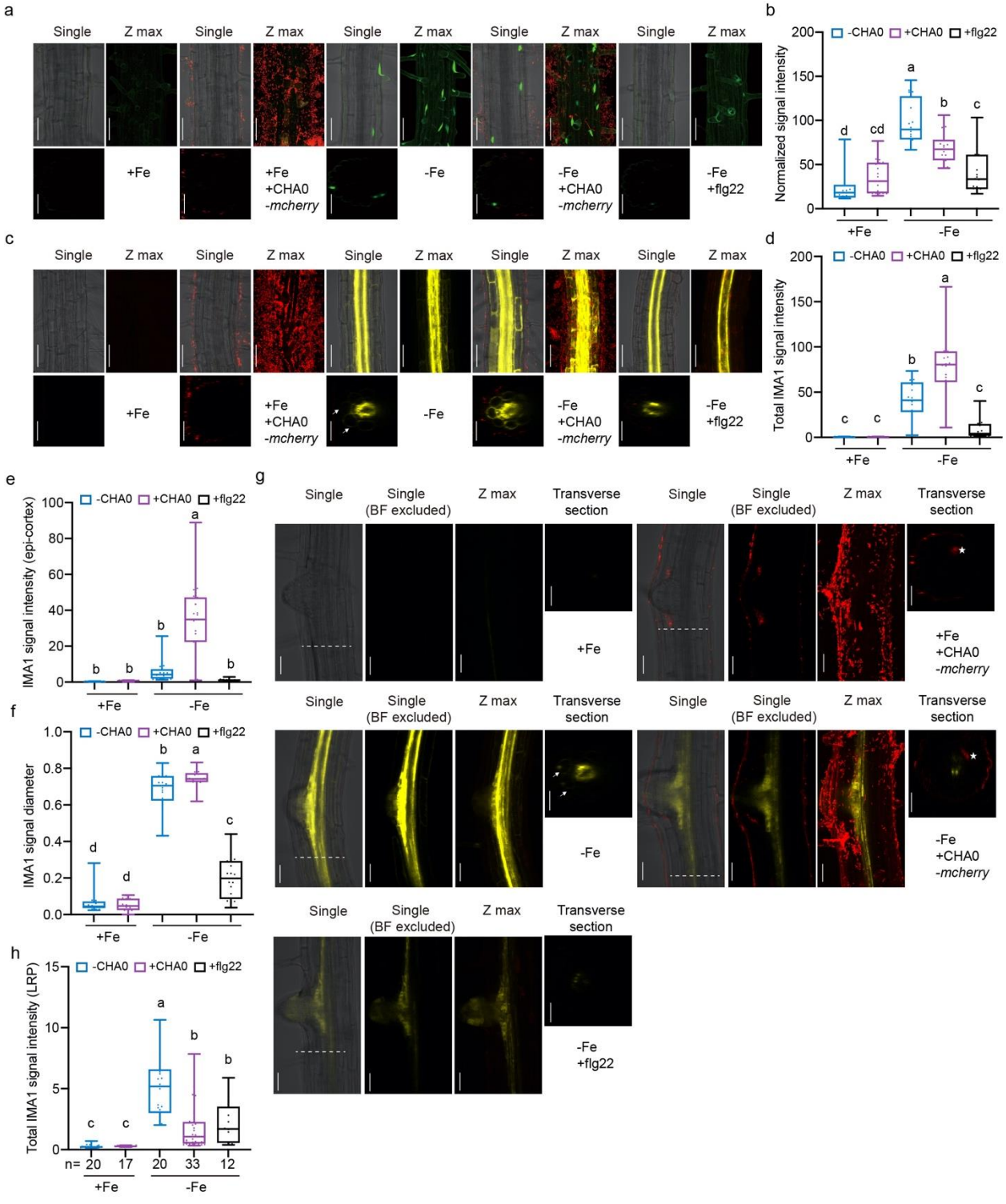
a
Single
Z max
+Fe
+Fe +CHA0 -mcherry
-Fe
-Fe +CHA0 -mcherry
-Fe +flg22
b
-CHA0
+CHA0
+flg22
Normalized signal intensity
+Fe
-Fe
c
Total IMA1 signal intensity
d
e
IMA1 signal intensity (epi-cortex)
f
IMA1 signal diameter
g
Single (BF excluded)
Transverse section
h
Total IMA1 signal intensity (LRP)
n= 20 17 20 33 12

Figure 6. IMA1 accumulation is distinctly modulated by surface dwelling or invading bacteria.
(a) The promoter activity of *IRT1* in the root of *pIRT1::NLS-2xYpet* seedlings in response to +Fe, +Fe+CHA0, -Fe, -Fe+CHA0 and -Fe+flg22 treatments. Cell surface localized CHA0-*mcherry* bacteria (red channel) and nuclear localized Ypet signals (green channel) are visualized with bright field microscopy. For each treatment, a representative single confocal section (single image, GFP/mCherry), a maximal Z-projection of the Z-stack (Z-max, GFP only) and a single optical section of the transverse view is shown. Scale bar, 50 µm.
(b) Normalized signal quantification of the promoter activity of *IRT1* in the root of *pIRT1::NLS-2xYpet* seedlings in response to +Fe, +Fe+CHA0, -Fe, -Fe+CHA0 and -Fe+flg22 treatments. Different letters indicate statistically significant differences between different conditions analyzed by one-way ANOVA and Fisher's LSD test($p<0.05$).
(c) IMA1 distribution in response to +Fe, +Fe+CHA0, -Fe, -Fe+CHA0 and -Fe+flg22 treatments in the differentiation zone of *pIMA1::EYFP-IMA1;ima8x* roots. The root surface localized CHA0-*mcherry* bacteria (red channel) and the cytosolic and nuclear localized EYFP-IMA1 signals (yellow channel) were visualized with bright field microscopy. For each treatment, a representative single confocal section (single image, EYFP/mCherry), a maximal Z-projection of the Z-stack (Z-max, EYFP only) and a single optical section of the transverse view is shown. Scale bar, 50 µm.
(d) Normalized IMA1 signal intensity quantification in response to +Fe, +Fe+CHA0, -Fe, -Fe+CHA0 and -Fe+flg22 treatments. Different letters indicate statistically significant differences between different conditions analyzed by one-way ANOVA and Fisher's LSD test($p<0.05$).
(e) Normalized IMA1 signal intensity in epidermis-cortex cell layers quantification in response to +Fe, +Fe+CHA0, -Fe, -Fe+CHA0 and -Fe+flg22 treatments. Different letters indicate statistically significant differences between different conditions analyzed by one-way ANOVA and Fisher's LSD test($p<0.05$).
(f) Normalized IMA1 signal diameter quantification in response to +Fe, +Fe+CHA0, -Fe, -Fe+CHA0 and -Fe+flg22 treatments. Different letters indicate statistically significant differences between different conditions analyzed by one-way ANOVA and Fisher's LSD test($p<0.05$).
(g) Representative images of EYFP-IMA1 in response to +Fe, +Fe+CHA0, -Fe, -Fe+CHA0 at emerging lateral root primordia. The interior localized CHA0-*mcherry* bacteria (Red channel) and the cytosolic and nuclear localized EYFP-IMA1 signals (yellow channel) are visualized with bright field. The asterisk indicates CHA0-*mcherry* colonized the inside of the root through the lateral root primordia site. The arrow shows weak IMA1 signal in the cortex. Scale bar, 50 µm. For each treatment, a single confocal section (single image, EYFP/mCherry), a maximal Z-projection of the Z-stack (Z-max, EYFP only) and a single optical section of the transverse view is shown. Scale bar, 50 µm.
(h) Normalized IMA1 signal intensity quantification in response to +Fe, +Fe+CHA0, -Fe, -Fe+CHA0 and -Fe+flg22 treatments at lateral root primordia region. Different letters indicate statistically significant differences between different conditions analyzed by one-way ANOVA and Fisher's LSD test($p<0.05$).

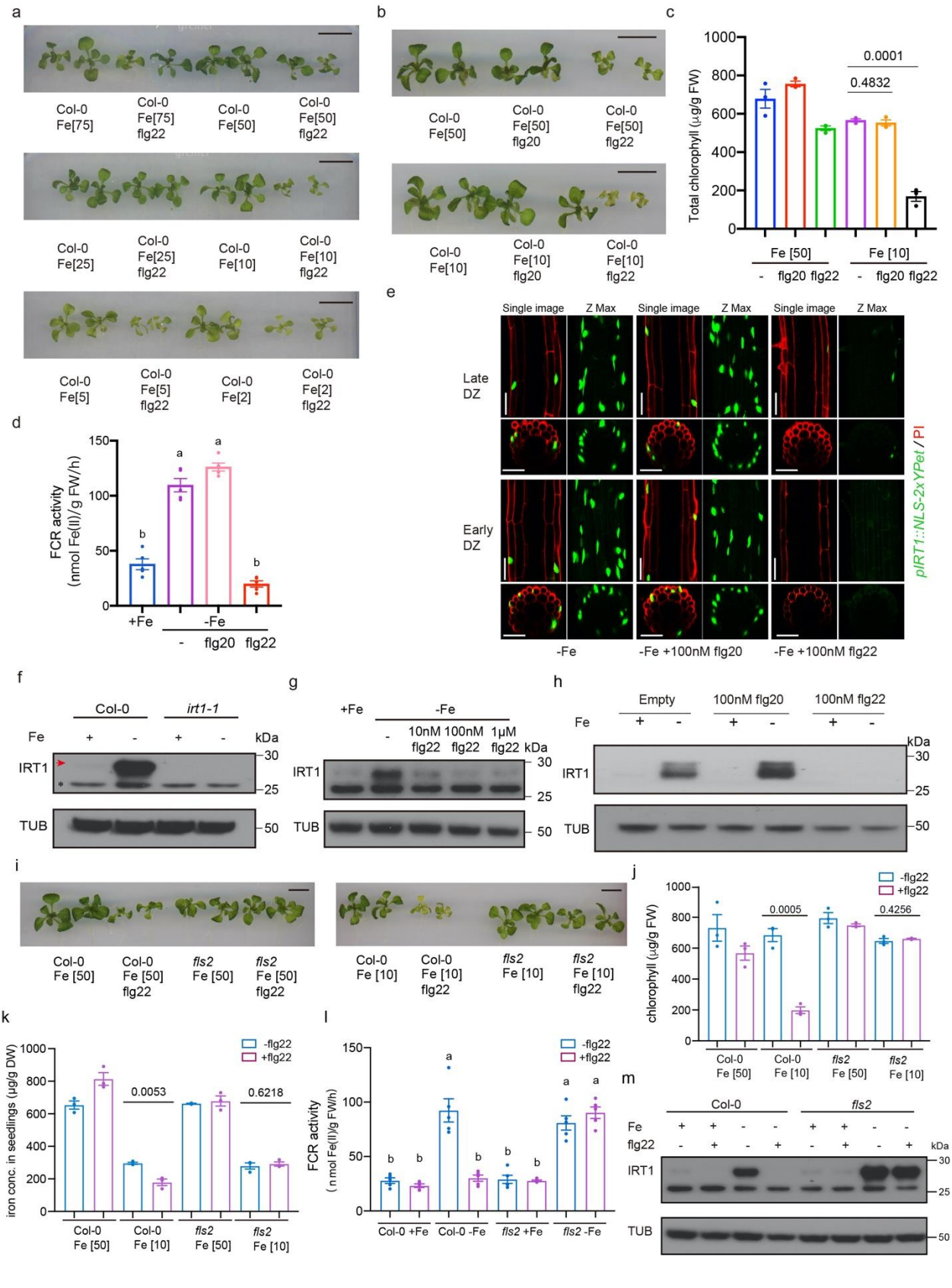
a
Col-0 Fe[75]
Col-0 Fe[75] flg22
Col-0 Fe[50]
Col-0 Fe[50] flg22
Col-0 Fe[25]
Col-0 Fe[25] flg22
Col-0 Fe[10]
Col-0 Fe[10] flg22
Col-0 Fe[5]
Col-0 Fe[5] flg22
Col-0 Fe[2]
Col-0 Fe[2] flg22
b
Col-0 Fe[50]
Col-0 Fe[50] flg20
Col-0 Fe[50] flg22
Col-0 Fe[10]
Col-0 Fe[10] flg20
Col-0 Fe[10] flg22
c
Total chlorophyll (µg/g FW)
0.0001
0.4832
Fe [50]
Fe [10]
- flg20 flg22 - flg20 flg22
d
FCR activity (nmol Fe(II)/g FW/h)
+Fe
-Fe
- flg20 flg22
e
Single image
Z Max
Late DZ
Early DZ
pIRT1::NLS-2xYPet / PI
-Fe
-Fe +100nM flg20
-Fe +100nM flg22
f
Col-0
irt1-1
Fe
kDa
IRT1
TUB
g
+Fe
-Fe
10nM flg22
100nM flg22
1µM flg22
h
Empty
100nM flg20
100nM flg22
i
Col-0 Fe [50]
Col-0 Fe [50] flg22
fls2 Fe [50]
fls2 Fe [50] flg22
Col-0 Fe [10]
Col-0 Fe [10] flg22
fls2 Fe [10]
fls2 Fe [10] flg22
j
-flg22
+flg22
chlorophyll (µg/g FW)
0.0005
0.4256
k
iron conc. in seedlings (µg/g DW)
0.0053
0.6218
l
FCR activity (n mol Fe(II)/g FW/h)
Col-0 +Fe
Col-0 -Fe
fls2 +Fe
fls2 -Fe
m
Col-0
fls2
flg22

Extended Data figure 1. Flg22 represses iron uptake through FLS2.
(a) Phenotype of 15-day-old Arabidopsis seedling leaves response to different iron concentration (shown in figures) with or without low levels of flg22 (10 nM) treatment. Scale bar 1cm.
(b-c) Phenotype of 15-day-old Arabidopsis seedling leaves response to sufficient iron (50 μM) or low iron (10 μM) with or without low levels of flg20 or flg22 (10 nM) treatment. The numbers correspond to P-values were analyzed by two-tailed Student t-test. (b) Shoots; Scale bar 1cm, (c) total chlorophyll concentration of Col-0 shoots. Bar chart centers show means of 3 biological replicates. Error bar: s.e.m.
(d) Quantitative analysis of ferric chelate reductase activities in Col-0 roots grown for 7 days under +Fe conditions and transferred to -Fe, -Fe with flg20 and -Fe with flg22 liquid medium for 2 days. The bar chart centers show means of 5 biological replicates. Error bar: s.e.m. Different letters indicate statistically significant differences between different conditions analyzed by one-way ANOVA and Tukey's test ($p<0.05$).
(e) Promoter activity of *IRT1* in the root of *pIRT1::NLS-2xYpet* seedlings in response to -Fe, -Fe with flg20 and -Fe with flg22 treatment. Seedlings were grown on the +Fe medium and after 5 days transferred to the different liquid media for 24 hours treatment. Green: Nuclear localized Ypet; Red: propidium iodide (PI) cell wall stain. For each treatment, a representative single confocal section (single image, GFP/PI), Maximum Intensity Z-Projection (Z-max, GFP only), a single optical section of the transverse view, and the Z-projection of the transverse section are shown. Scale bar, 50 μm.
(f-h) Western blots showing IRT1 protein levels in Col-0 and *irt1-1* roots grown in +Fe and -Fe (e) or Col-0 under +Fe, -Fe and -Fe with different concentrations of flg22 treatment (f) or Col-0 under +Fe, -Fe and -Fe with flg20 or flg22 treatment (h). Arrow indicates the IRT1 protein band. The asterisk indicates non-specific band. Tubulin protein was blotted as an internal control.
(i-k) Phenotype of 15-day-old Arabidopsis Col-0 and *fls2* seedling leaves response to sufficient iron (50 μM) or low iron (10 μM) with or without low levels of flg22 (10 nM) treatment. The numbers correspond to P-values were analyzed by two-tailed Student t-test. (i) Shoots; Scale bar 1cm, (j) total chlorophyll concentration of Col-0 shoots, (k) Iron concentration of Col-0 seedlings; bar chart centers show means of 3 biological replicates. Error bar: s.e.m.
(l) Quantitative analysis of ferric chelate reductase activities in Col-0 and *fls2* roots grown for 7 days under +Fe conditions and transferred to +Fe, +Fe with flg22, -Fe and -Fe with flg22 liquid medium for 2 days. The bar chart centers show means of 5 biological replicates. Error bar: s.e.m. Different letters indicate statistically significant differences between different conditions analyzed by one-way ANOVA and Tukey's test ($p<0.05$).
(m) Western blots showing IRT1 protein levels in Col-0 and *fls2* roots in +Fe, +Fe with flg22, -Fe and -Fe with flg22 treatment. The tubulin protein was blotted as an internal control.

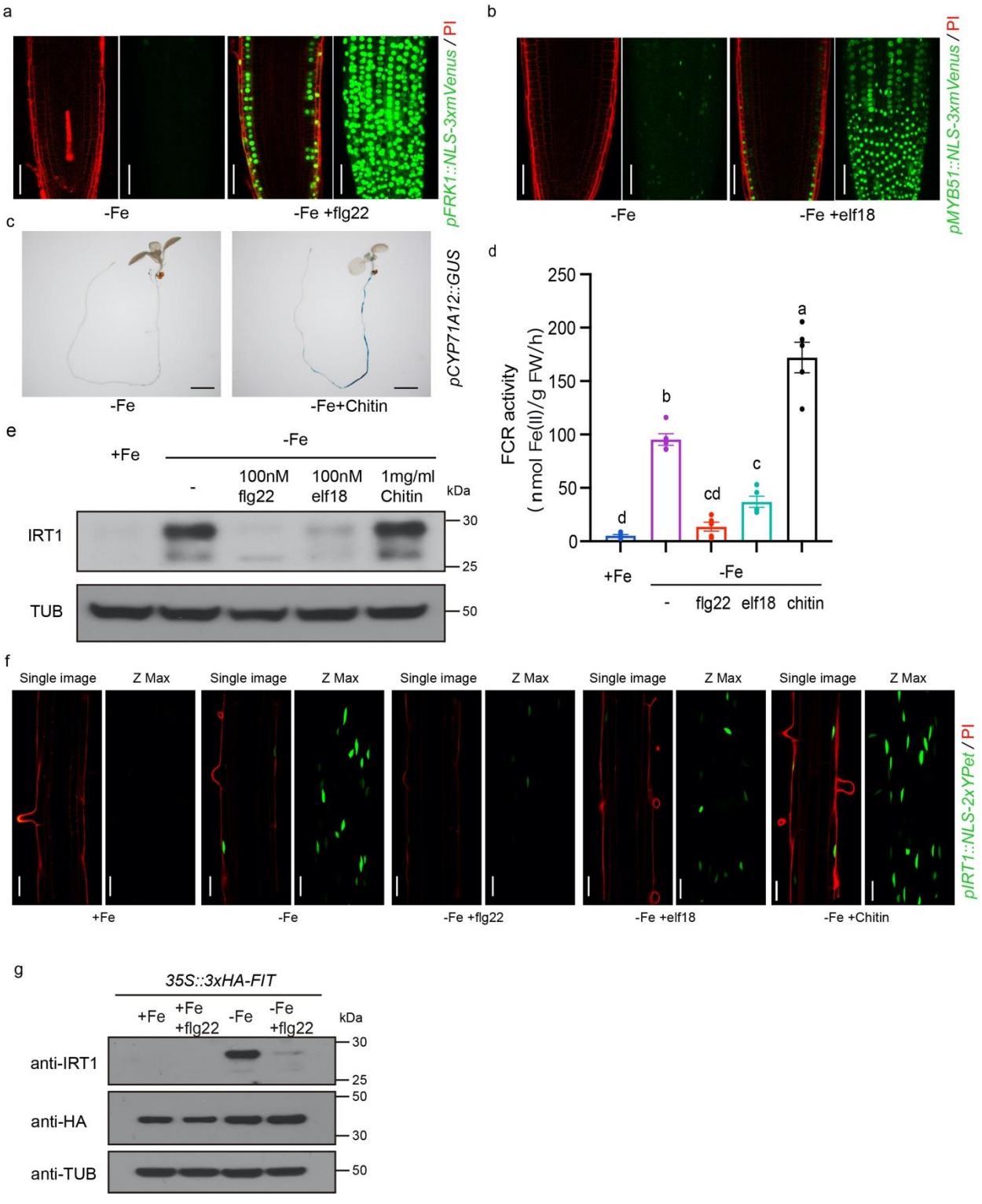
a
pFRK1::NLS-3xmVenus / PI
-Fe
-Fe +flg22
b
pMYB51::NLS-3xmVenus / PI
-Fe
-Fe +elf18
c
pCYP71A12::GUS
-Fe
-Fe+Chitin
d
FCR activity
(nmol Fe(II)/g FW/h)
250
200
150
100
50
0
a
b
cd
c
d
+Fe
-Fe
-
flg22
elf18
chitin
e
+Fe
-Fe
-
100nM flg22
100nM elf18
1mg/ml Chitin
kDa
IRT1
TUB
30
25
50
f
Single image
Z Max
pIRT1::NLS-2xYPet / PI
+Fe
-Fe
-Fe +flg22
-Fe +elf18
-Fe +Chitin
g
35S::3xHA-FIT
+Fe
+Fe +flg22
-Fe
-Fe +flg22
kDa
anti-IRT1
anti-HA
anti-TUB
30
25
50
30
50

Extended Data figure 2. MAMPs regulate iron uptake through distinct mechanisms.
(a-b) Promoter activity of *FRK1* in roots of *pFRK1::NLS-3xmVenus* seedlings in response to -Fe and -Fe with flg22 treatment (a) or Promoter activity of *MYB51* in roots of *pMYB51::NLS-3xmVenus* seedlings in response to -Fe and -Fe with elf18 treatment (b). 7-day-old seedlings are treated with -Fe and -Fe with 100nM flg22 (a) or -Fe and -Fe with 100nM elf18 (b) for 24 hours in liquid media. Green: Nuclear localized mVenus signals; Red: propidium iodide (PI) cell wall stain. In each treatment, a representative single confocal section (single image, GFP/PI) and Maximum Intensity Z-Projection (Z-max, GFP only) is shown. Scale bar, 50 µm.
(c) Promoter activity of *CYP71A12* in roots of *pCYP71A12::GUS* seedlings in response to -Fe and -Fe with Chitin treatment. 7-day-old seedlings are treated with -Fe and -Fe with 1mg/mL for 24 hours in liquid media. Scale bar, 0.5cm.
(d) Quantitative analysis of ferric chelate reductase activities in Col-0 roots grown for 7 days under +Fe conditions and transferred to -Fe, -Fe only or -Fe with flg22, elf18 and Chitin liquid medium for 2 days. The bar chart centers show means of 5 biological replicates. Error bars, s.e.m. Different letters indicate statistically significant differences between different conditions analyzed by one-way ANOVA and Tukey's test ($p<0.05$).
(e) Western blots showing IRT1 protein levels in Col-0 roots grown +Fe, -Fe only or -Fe with flg22, elf18 and chitin treatment. Tubulin protein was blotted as an internal control.
(f) Promoter activity of *IRT1* in the root of *pIRT1::NLS-2xYpet* seedlings in response to -Fe only or -Fe with flg22, elf18 and Chitin treatment. Green: Nuclear localized Ypet signals; Red: propidium iodide (PI) cell wall stain. In each treatment, the Z-stack scan is processed to single confocal section (single image, GFP/PI), maximal Z-projection (Z-max, GFP only). Scale bar, 50 µm.
(g) Western blots showing IRT1 protein levels in *35S::3xHA-FIT* roots is in response to +Fe, +Fe with flg22, -Fe and -Fe with flg22 treatment. HA tagged FIT protein was blotted using anti-HA antibody. Tubulin protein was blotted as an internal control.

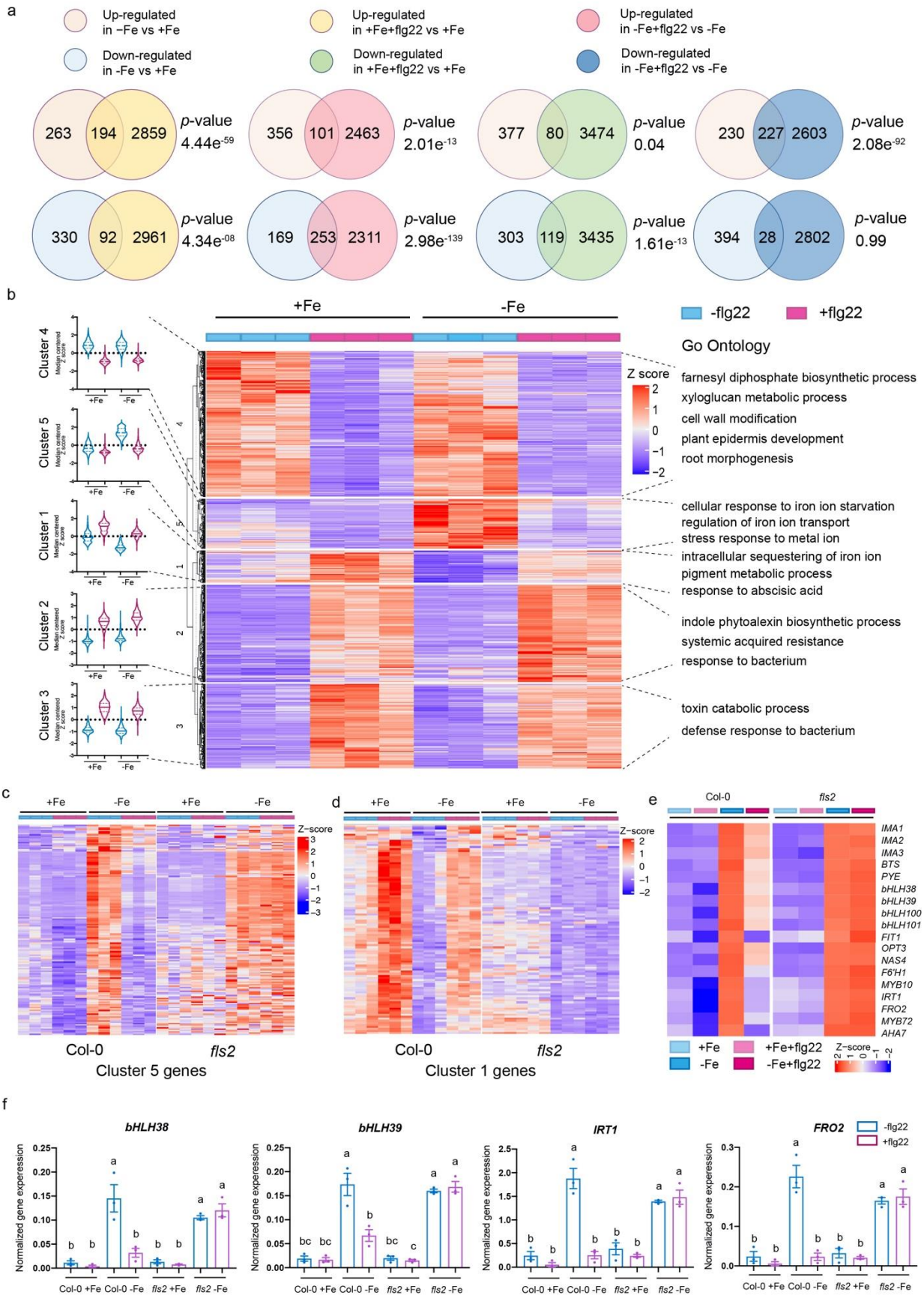
a
Up-regulated in −Fe vs +Fe
Down-regulated in -Fe vs +Fe
Up-regulated in +Fe+flg22 vs +Fe
Down-regulated in +Fe+flg22 vs +Fe
Up-regulated in -Fe+flg22 vs -Fe
Down-regulated in -Fe+flg22 vs -Fe
263 194 2859 p-value 4.44e-59
356 101 2463 p-value 2.01e-13
377 80 3474 p-value 0.04
230 227 2603 p-value 2.08e-92
330 92 2961 p-value 4.34e-08
169 253 2311 p-value 2.98e-139
303 119 3435 p-value 1.61e-13
394 28 2802 p-value 0.99
b
+Fe
-Fe
-flg22
+flg22
Go Ontology
Cluster 4
Cluster 5
Cluster 1
Cluster 2
Cluster 3
Z score
farnesyl diphosphate biosynthetic process
xyloglucan metabolic process
cell wall modification
plant epidermis development
root morphogenesis
cellular response to iron ion starvation
regulation of iron ion transport
stress response to metal ion
intracellular sequestering of iron ion
pigment metabolic process
response to abscisic acid
indole phytoalexin biosynthetic process
systemic acquired resistance
response to bacterium
toxin catabolic process
defense response to bacterium
c
Z−score
Col-0
fls2
Cluster 5 genes
d
Z−score
Col-0
fls2
Cluster 1 genes
e
Col-0
fls2
IMA1
IMA2
IMA3
BTS
PYE
bHLH38
bHLH39
bHLH100
bHLH101
FIT1
OPT3
NAS4
F6'H1
MYB10
IRT1
FRO2
MYB72
AHA7
+Fe
-Fe
+Fe+flg22
-Fe+flg22
Z−score
f
bHLH38
bHLH39
IRT1
FRO2
-flg22
+flg22
Normalized gene expression
Col-0 +Fe
Col-0 -Fe
fls2 +Fe
fls2 -Fe

Extended Data figure 3. Flg22 antagonistically regulates the iron deficiency transcriptional landscape through FLS2.

(a) Venn diagram of up/down-regulated genes of +Fe+flg22 vs +Fe, -Fe vs +Fe and -Fe+flg22 vs -Fe, respectively. The statistical analysis of *p*-value was calculated by hypergeometric test.

(b) Heat map of mean-centered Z-scores for 1290 differentially expressed genes identified across different treatment (+Fe, +Fe+flg22, -Fe and -Fe+flg22), arranged by *k*-means clustering. Box plot indicates the relative expression level based on median centered Z-score in different clusters. The GO terms analysis was performed using PANTHER17.0 (p-value<0.05) and indicated on the right side of the heatmap.

(c&d) Heat map of mean-centered Z-scores for differentially expressed genes (cluster 5 (c) and cluster 1 (d) in WT and *fls2*) identified across different treatments (+Fe, +Fe+flg22, -Fe and -Fe+flg22), arranged by *k*-means clustering.

(e) Heat map of mean-centered Z-scores (normalized by Col-0 +Fe) for well-known iron responsive genes in response to +Fe, +Fe+flg22, -Fe and -Fe+flg22 in Col-0 and *fls2* roots.

(f) Gene expression analysis in response to +Fe, +Fe with flg22, -Fe and -Fe with flg22 treatment in Col-0 and *fls2* roots by quantitative RT-PCR. The gene expression level is normalized to *ACT2* internal control. The bar chart centers show means of 3 biological replicates. Error bars, s.e.m. Different letters indicate statistically significant differences between different conditions analyzed by one-way ANOVA and Tukey's test ($p<0.05$).

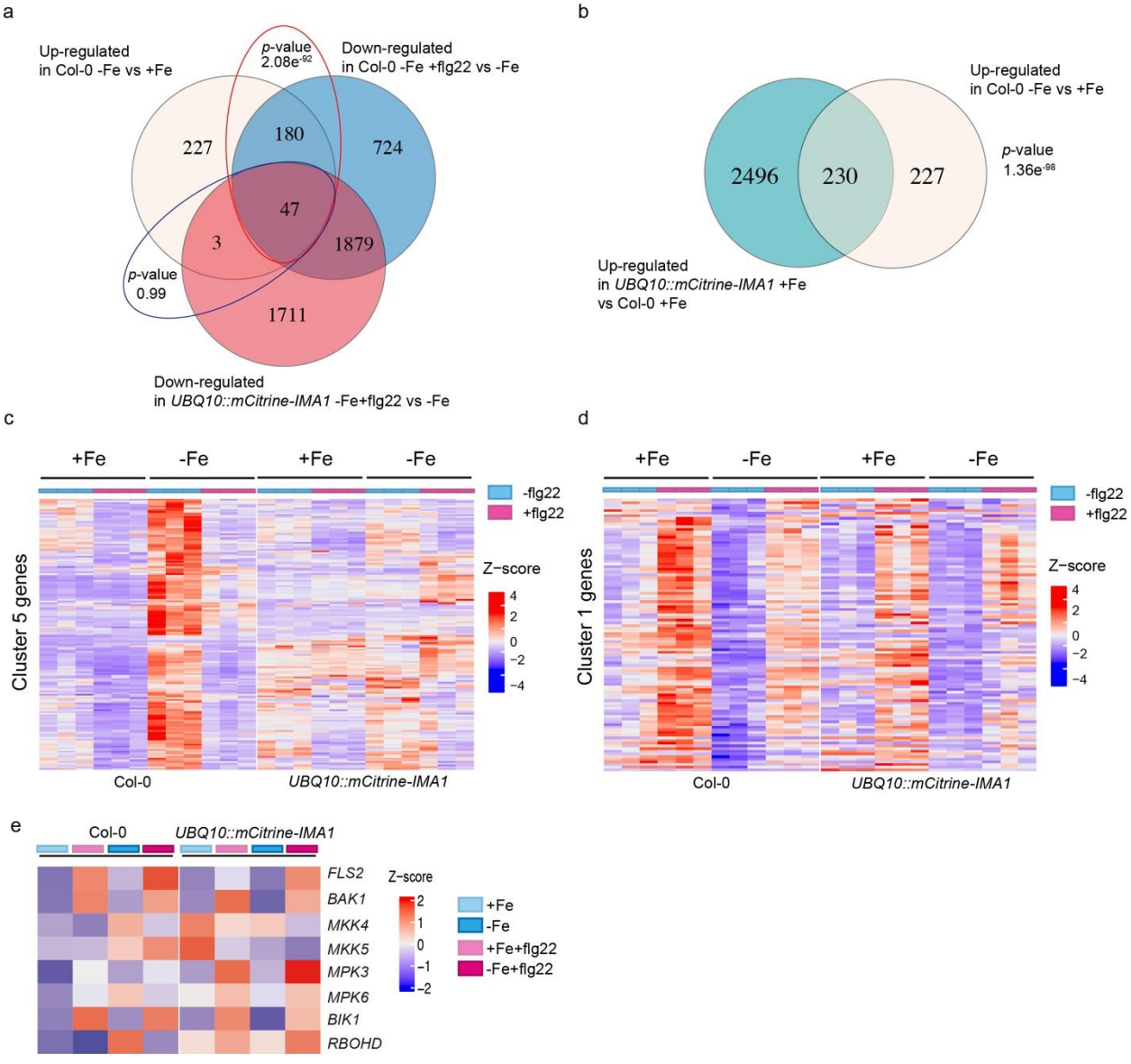
a
Up-regulated
in Col-0 -Fe vs +Fe
p-value
2.08e-92
Down-regulated
in Col-0 -Fe +flg22 vs -Fe
227
180
724
47
3
1879
p-value
0.99
1711
Down-regulated
in UBQ10::mCitrine-IMA1 -Fe+flg22 vs -Fe
b
Up-regulated
in Col-0 -Fe vs +Fe
p-value
1.36e-98
2496
230
227
Up-regulated
in UBQ10::mCitrine-IMA1 +Fe
vs Col-0 +Fe
c
+Fe
-Fe
+Fe
-Fe
-flg22
+flg22
Z−score
4
2
0
−2
−4
Cluster 5 genes
Col-0
UBQ10::mCitrine-IMA1
d
+Fe
-Fe
+Fe
-Fe
-flg22
+flg22
Z−score
4
2
0
−2
−4
Cluster 1 genes
Col-0
UBQ10::mCitrine-IMA1
e
Col-0
UBQ10::mCitrine-IMA1
FLS2
BAK1
MKK4
MKK5
MPK3
MPK6
BIK1
RBOHD
Z−score
2
1
0
−1
−2
+Fe
-Fe
+Fe+flg22
-Fe+flg22

Extended Data figure 4. Flg22 antagonistically regulates the iron deficiency transcriptional landscape through IMA1.

(a&b) Venn diagram of the iron deficiency up-regulated genes in Col-0 vs down-regulated genes of -Fe+flg22 vs -Fe in Col-0 vs down-regulated genes of -Fe+flg22 vs -Fe in *UBQ10::mCitrine-IMA1* (a). Venn diagram of the iron deficiency up-regulated genes in Col-0 vs upregulated genes in *UBQ10::mCitrine-IMA1* in +Fe vs Col-0 +Fe (b). The statistical analysis of *p*-value was calculated by hypergeometric test.

(c&d) Heat map of mean-centered Z-scores for differentially expressed genes (cluster 5 and cluster 1 in WT and *UBQ10::mCitine-IMA1*) identified across different treatments (+Fe, +Fe+flg22, -Fe and -Fe+flg22), arranged by *k*-means clustering.

(e) Heat map of mean-centered Z-scores (normalized by Col-0 +Fe) for well-known PTI components in response to +Fe, +Fe+flg22, -Fe and -Fe+flg22, respectively.

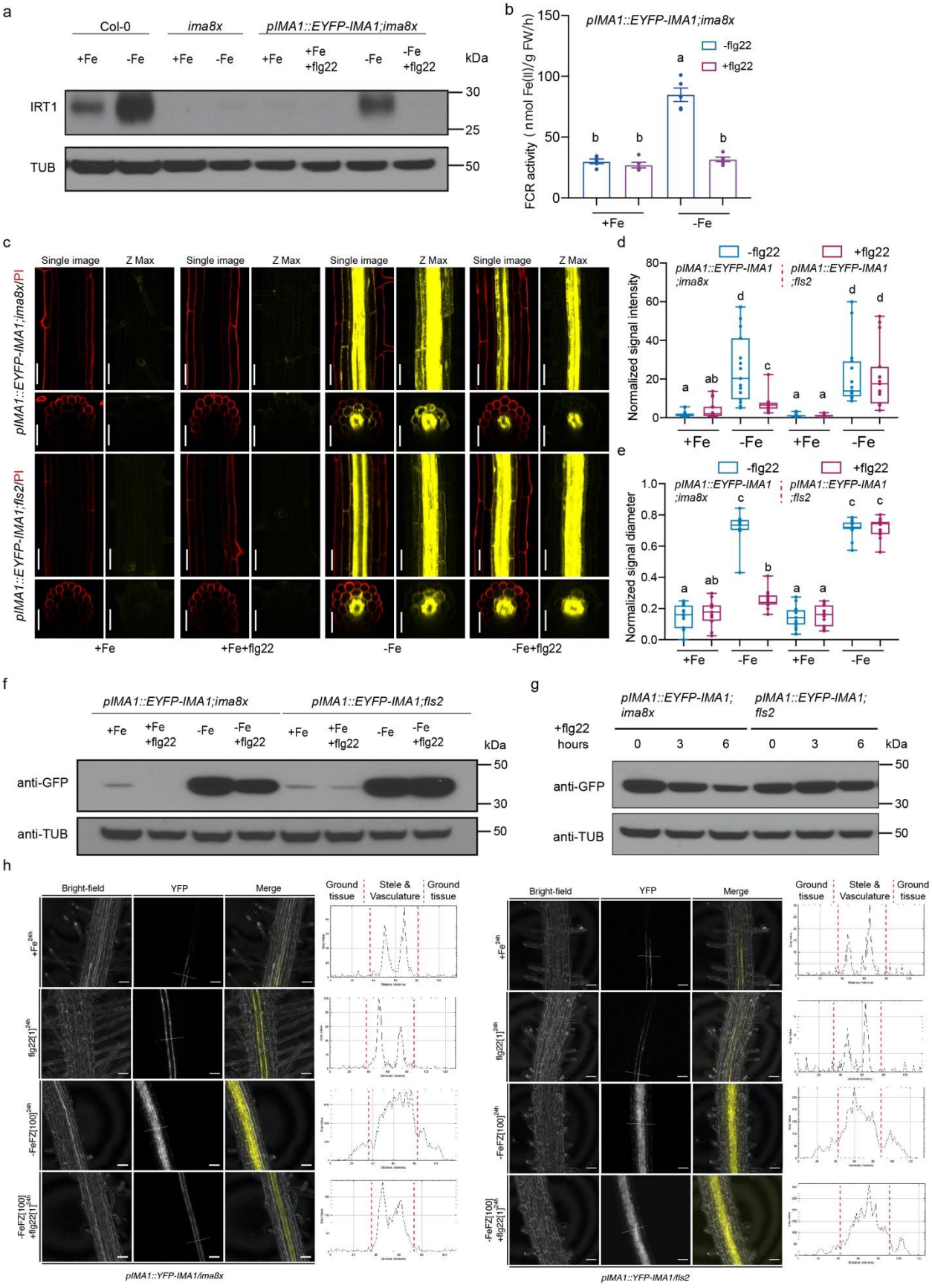
a
Col-0
ima8x
pIMA1::EYFP-IMA1;ima8x
+Fe
-Fe
+Fe +flg22
-Fe +flg22
kDa
IRT1
TUB
30
25
50
b
pIMA1::EYFP-IMA1;ima8x
-flg22
+flg22
FCR activity (nmol Fe(III)/g FW/h)
150
100
50
0
c
Single image
Z Max
pIMA1::EYFP-IMA1;ima8x/PI
pIMA1::EYFP-IMA1;fls2/PI
+Fe
+Fe+flg22
-Fe
-Fe+flg22
d
pIMA1::EYFP-IMA1 ;ima8x
pIMA1::EYFP-IMA1 ;fls2
Normalized signal intensity
e
Normalized signal diameter
f
anti-GFP
anti-TUB
g
+flg22 hours
0
3
6
h
Bright-field
YFP
Merge
Ground tissue
Stele & Vasculature
+Fe24h
flg22[1]24h
-FeFZ[100]24h
-FeFZ[100] +flg22[1]24h
pIMA1::YFP-IMA1/ima8x
pIMA1::YFP-IMA1/fls2

Extended Data figure 5. flg22 spatially regulates IMA1 protein level in the ground tissue of the root through FLS2.

(a) Western blots showing IRT1 protein levels in Col-0, *ima8x* and *pIMA1::EYFP-IMA1;ima8x* in different treatment conditions. Seedlings were treated with +Fe and -Fe (Col-0 and *ima8x*) and +Fe, +Fe with flg22, -Fe and -Fe with flg22 treatment (*pIMA1::EYFP-IMA1;ima8x*). Tubulin protein was blotted as an internal control.

(b) Quantitative analysis of ferric chelate reductase activities in *pIMA1::EYFP-IMA1;ima8x* roots grown for 7 days under +Fe conditions and transferred to +Fe, +Fe with flg22, -Fe and -Fe with flg22 liquid medium for 2 days. The bar chart centers show mean of 5 biological replicates. Error bars, s.e.m. Different letters indicate statistically significant differences between different conditions analyzed by one-way ANOVA and Tukey's test ($p<0.05$).

(c) IMA1 distribution in response to +Fe, +Fe with flg22, -Fe and -Fe with flg22 treatment in differentiation zone of the root. 5 days old *pIMA1::EYFP-IMA1;ima8x* and *pIMA1::EYFP-IMA1;fls2* seedlings were grown on the +Fe medium and then transferred to different liquid media for 24 hours treatment. The cytosolic and nuclear localized EYFP-IMA1 signals (yellow channel) are visualized with propidium iodide (PI, cell wall staining, red channel). For each treatment, a representative single confocal section (single image, EYFP/PI), a maximal Z-projection of the Z-stack (Z-max, EYFP only), a single optical section of the transverse view, and the Z-projection of the transverse section is shown. Scale bar, 50 μm.

(d-e) Quantification of IMA1 fluorescence signal intensity (d) and normalized IMA1 signal diameter (e) in response to +Fe, +Fe with flg22, -Fe and -Fe with flg22 treatment in differentiation zone of the root in *pIMA1::EYFP-IMA1;ima8x* and *pIMA1::EYFP-IMA1;fls2* (n=15 biologically independent seedlings). The same dataset from Figure 3d&f of *pIMA1::EYFP-IMA1;ima8x* were used here as the images for quantification were taken at the same time. Different letters indicate statistically significant differences between different conditions analyzed by Multiple pairwise comparisons using the Steel-Dwass-Critchlow-Fligner procedure / Two-tailed test($p<0.05$).

(f) Western blots showing IMA1 protein levels in the roots of *pIMA1::EYFP-IMA1;ima8x* and *pIMA1::EYFP-IMA1;fls2* in +Fe, +Fe with flg22, -Fe and -Fe with flg22 treatments. Tubulin protein was blotted as an internal control.

(g) Western blots showing IMA1 protein levels in *pIMA1::EYFP-IMA1;ima8x* and *pIMA1::EYFP-IMA1;fls2* roots. The seedlings were pre-treatment with -Fe for 36 hours, then treated with -Fe+flg22 (1μm flg22) for 0, 3 and 6 hours. Tubulin protein was blotted as an internal control.

(h) Representative image of EYFP-IMA1 signal intensity profile in response to +Fe, +Fe with flg22, -Fe and -Fe with flg22 treatment in differentiation zone of root in *pIMA1::EYFP-IMA1;ima8x* (left panel) and *pIMA1::EYFP-IMA1;fls2* (right panel). The white line in YFP channel indicates the line for signal quantification. The red dashed lines indicate the boundary between the ground tissue and the stele. Scale bar, 50 μm.

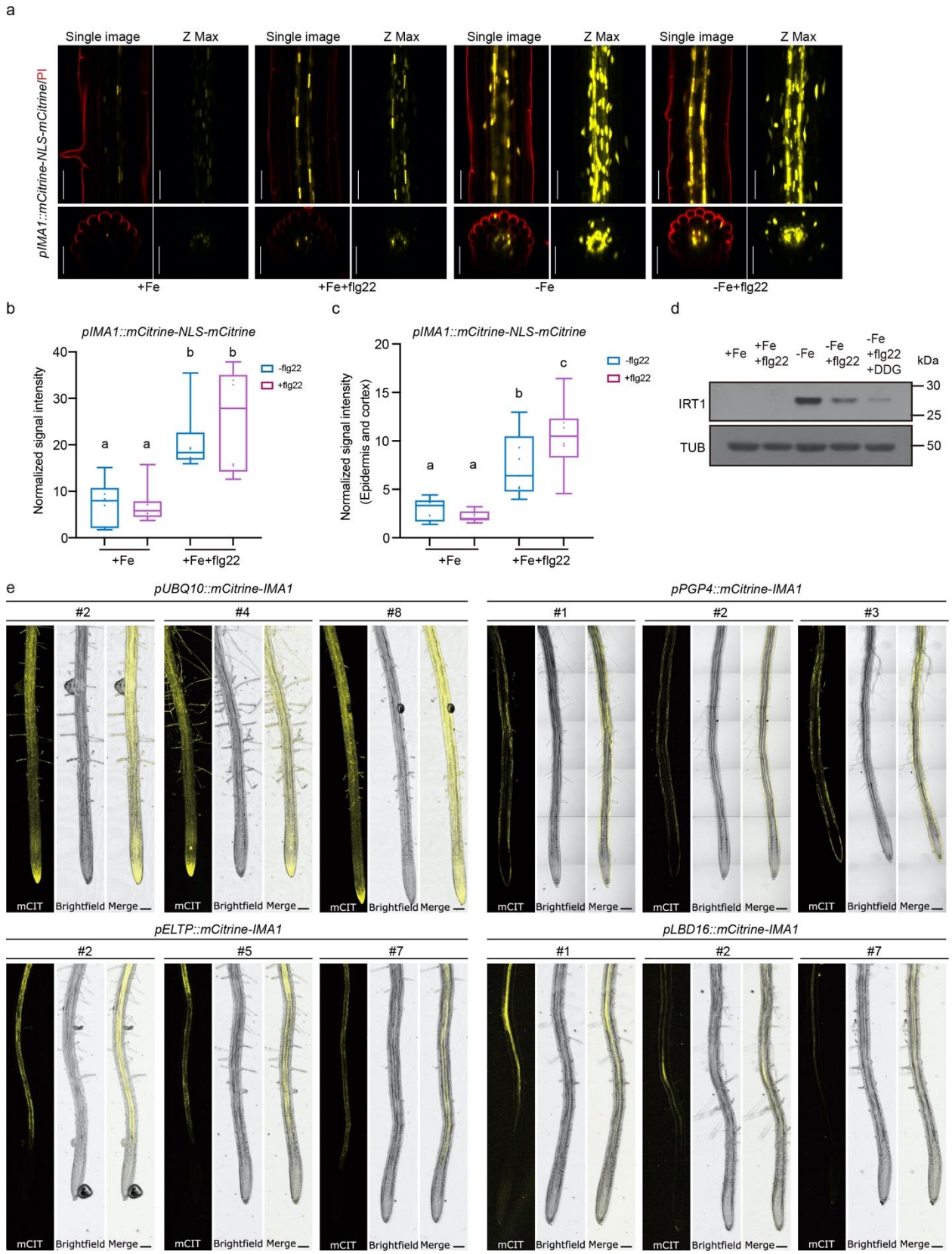
a
Single image
Z Max
pIMA1::mCitrine-NLS-mCitrine/PI
+Fe
+Fe+flg22
-Fe
-Fe+flg22
b
pIMA1::mCitrine-NLS-mCitrine
Normalized signal intensity
-flg22
+flg22
c
pIMA1::mCitrine-NLS-mCitrine
Normalized signal intensity (Epidermis and cortex)
d
+Fe
+Fe +flg22
-Fe
-Fe +flg22
-Fe +flg22 +DDG
kDa
IRT1
TUB
e
pUBQ10::mCitrine-IMA1
pPGP4::mCitrine-IMA1
pELTP::mCitrine-IMA1
pLBD16::mCitrine-IMA1
mCIT
Brightfield
Merge

Extended Data figure 6. flg22 does not fully repress *IMA1* transcription in the ground tissue and flg22 dependent callose deposition is not required for IRT1 repression.

(a) Promoter activity of *IMA1* in the root of *pIMA1::mCitrine-NLS-mCitrine* seedlings in response to +Fe, +Fe with flg22, -Fe and -Fe with flg22 treatment. 5-day-old seedlings were grown on the +Fe medium and then transferred to the different liquid media for 24 hours treatment. The nuclear localized mCitrine signals (Yellow channel) are visualized with propidium iodide (PI, Red channel). For each treatment, a representative single confocal section (single image, GFP/PI), Maximum Intensity Z-Projection (Z-max, GFP only), a single optical section of the transverse view, and the Z-projection of the transverse section is shown. Scale bar, 50 μm.

(b-c) Normalized IMA1 promoter activity quantification in all cell layers (b) or in epidermis-cortex cell layers (c) in response to +Fe, +Fe+flg22, -Fe and -Fe+flg22 treatments. Different letters indicate statistically significant differences between different conditions analyzed by one-way ANOVA and Fisher's LSD test($p<0.05$).

(d) Western blots showing IRT1 protein levels in Col-0 roots is in response to +Fe, +Fe with flg22, -Fe, -Fe with flg22 treatment and -Fe with flg22 and DDG treatment. Tubulin protein was blotted as an internal control.

(e) Representative images of cell-layer specific IMA1 expression transgenic plants. 3 individual lines were shown under +Fe condition. Scale bar, 100 μm.

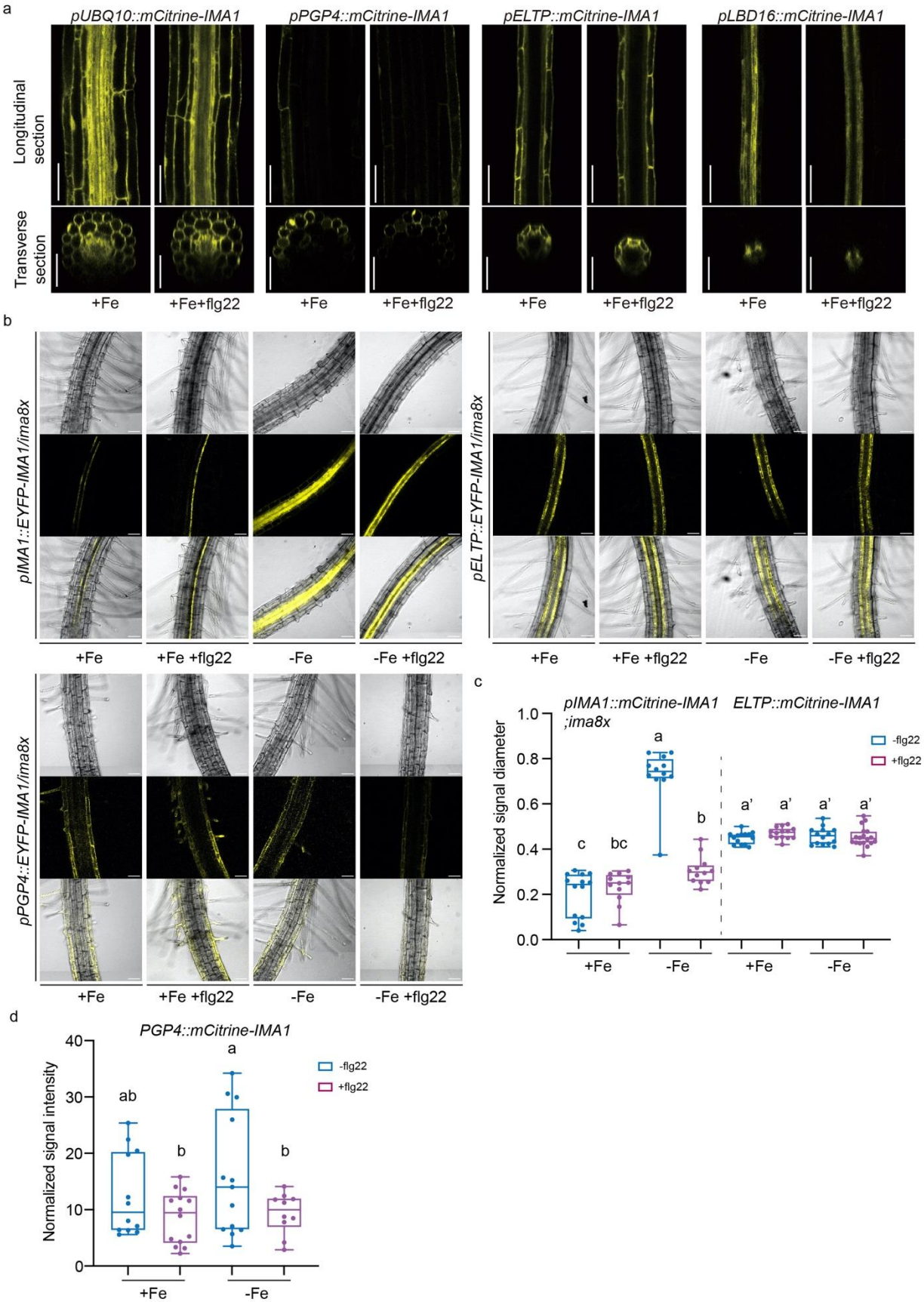
a
pUBQ10::mCitrine-IMA1
pPGP4::mCitrine-IMA1
pELTP::mCitrine-IMA1
pLBD16::mCitrine-IMA1
Longitudinal section
Transverse section
+Fe
+Fe+flg22
b
pIMA1::EYFP-IMA1/ima8x
pELTP::EYFP-IMA1/ima8x
pPGP4::EYFP-IMA1/ima8x
+Fe
+Fe +flg22
-Fe
-Fe +flg22
c
pIMA1::mCitrine-IMA1 ;ima8x
ELTP::mCitrine-IMA1
Normalized signal diameter
-flg22
+flg22
a
b
c
bc
a'
+Fe
-Fe
d
PGP4::mCitrine-IMA1
Normalized signal intensity
ab
b
a
b

Extended Data figure 7. IMA1 is not regulated through cell-to-cell movement but regulated through protein level in the epidermis-cortex under -Fe by flg22.

(a) Representative images of roots of plants with different tissue-specific promoters driving IMA1 expression. 5-day-old transgenic seedlings were grown on +Fe solid medium and then transferred to +Fe or +Fe+flg22 liquid medium for 24 hours treatment. For each treatment, the cytosolic and nuclear-localized mCitrine-IMA1 signals (yellow channel) are visualized with longitudinal section and transverse section. Scale bar, 50 μm.

(b) Representative images of roots of plants with *pIMA1*, *pELTP* or *pPGP4* promoters driving IMA1 expression in response to +Fe, +Fe+flg22, -Fe and -Fe+flg22. For each treatment, mCitrine-IMA1 signals (yellow channel) and bright field are visualized with longitudinal section. Scale bar, 50 μm.

(c) Quantification of normalized IMA1 signal diameter in different treatment conditions in differentiation zones of the roots. Different letters indicate statistically significant differences between different conditions analyzed by one-way ANOVA and Fisher's LSD test($p<0.05$).

(d) Quantification of normalized IMA1 signal intensity of *pPGP4::mCitrine-IMA1* in different treatment conditions. Different letters indicate statistically significant differences between different conditions analyzed by one-way ANOVA and Fisher's LSD test($p<0.05$).

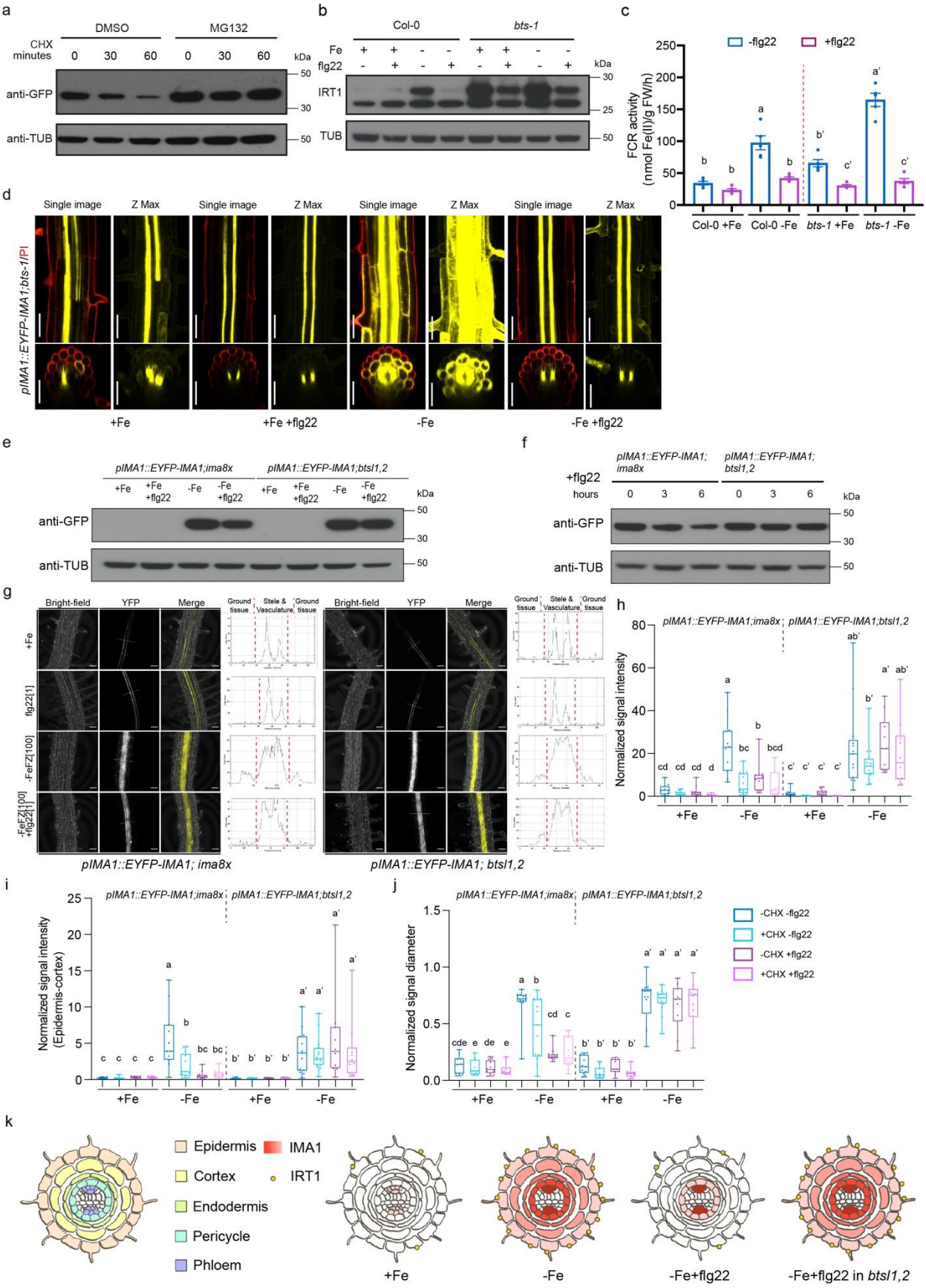
a
DMSO
MG132
CHX
minutes
0
30
60
0
30
60
kDa
anti-GFP
anti-TUB
50
30
50
b
Col-0
bts-1
Fe
flg22
IRT1
TUB
kDa
30
25
50
c
-flg22
+flg22
FCR activity
(nmol Fe(II)/g FW/h)
250
200
150
100
50
0
Col-0 +Fe
Col-0 -Fe
bts-1 +Fe
bts-1 -Fe
d
Single image
Z Max
pIMA1::EYFP-IMA1;bts-1/PI
+Fe
+Fe +flg22
-Fe
-Fe +flg22
e
pIMA1::EYFP-IMA1;ima8x
pIMA1::EYFP-IMA1;btsl1,2
+Fe
+Fe +flg22
-Fe
-Fe +flg22
kDa
anti-GFP
anti-TUB
50
30
50
f
+flg22
hours
pIMA1::EYFP-IMA1; ima8x
pIMA1::EYFP-IMA1; btsl1,2
0
3
6
0
3
6
kDa
anti-GFP
anti-TUB
50
30
50
g
Bright-field
YFP
Merge
Ground tissue
Stele & Vasculature
Ground tissue
+Fe
flg22[1]
-FeFZ[100]
-FeFZ[100] +flg22[1]
pIMA1::EYFP-IMA1; ima8x
pIMA1::EYFP-IMA1; btsl1,2
h
pIMA1::EYFP-IMA1;ima8x
pIMA1::EYFP-IMA1;btsl1,2
Normalized signal intensity
80
60
40
20
0
+Fe
-Fe
+Fe
-Fe
i
pIMA1::EYFP-IMA1;ima8x
pIMA1::EYFP-IMA1;btsl1,2
Normalized signal intensity
(Epidermis-cortex)
25
20
15
10
5
0
+Fe
-Fe
+Fe
-Fe
j
pIMA1::EYFP-IMA1;ima8x
pIMA1::EYFP-IMA1;btsl1,2
Normalized signal diameter
1.5
1.0
0.5
0.0
+Fe
-Fe
+Fe
-Fe
-CHX -flg22
+CHX -flg22
-CHX +flg22
+CHX +flg22
k
Epidermis
Cortex
Endodermis
Pericycle
Phloem
IMA1
IRT1
+Fe
-Fe
-Fe+flg22
-Fe+flg22 in btsl1,2

Extended Data figure 8. flg22 dependent IMA1 degradation in the ground tissue is regulated by BTSL1 and BTSL2 but not by BTS.

(a) Western blots showing IMA1 protein is degraded through ubiquitin-dependent proteasome mechanism under -Fe condition. The *pIMA1::EYFP-IMA1;ima8x* was pretreat with -Fe with DMSO only or -Fe with 10 μM MG132 for 36 hours, subsequently with 100 μM Cycloheximide (CHX) with indicated time period. Tubulin protein was blotted as an internal control.

(b) Western blots showing IRT1 protein levels in Col-0 and *bts-1* roots in +Fe, +Fe with flg22, -Fe and -Fe with flg22 treatment. Tubulin protein was blotted as an internal control.

(c) Quantitative analysis of Ferric Reductase activities in Col-0 and *bts-1* roots grown for 7 days under +Fe conditions and transferred to +Fe, +Fe with flg22, -Fe and -Fe with flg22 liquid medium for 2 days. The bar chart centers show mean of 5 biological replicates. Error bars, s.e.m. Different letters indicate statistically significant differences between different conditions analyzed by one-way ANOVA and Tukey's test ($p<0.05$).

(d) IMA1 distribution in *bts-1* in response to +Fe, +Fe with flg22, -Fe and -Fe with flg22 treatment in differentiation zone of the root. 5 days old *pIMA1::EYFP-IMA1;bts-1* seedlings were grown on the +Fe medium and then transferred to different liquid medium for 24 hours treatment. The cytosolic and nuclear localized EYFP-IMA1 signals (yellow channel) are visualized with propidium iodide (PI, red channel). For each treatment, a representative single confocal section (single image, EYFP/PI), a maximal Z-projection of the Z-stack (Z-max, EYFP only), a single optical section of the transverse view, and the Z-projection of the transverse section is shown. Scale bar, 50 μm.

(e) Western blots showing IMA1 protein levels in the roots of *pIMA1::EYFP-IMA1;ima8x* and *pIMA1::EYFP-IMA1;btsl1,2* in +Fe, +Fe with flg22, -Fe and -Fe with flg22 treatments. Tubulin protein was blotted as an internal control.

(f) Western blots showing IMA1 protein levels in *pIMA1::EYFP-IMA1;ima8x* and *pIMA1::EYFP-IMA1;btsl1,2* roots. The seedlings were pre-treatment with -Fe for 36 hours, then treated with -Fe+flg22 (1μm flg22) for 0, 3 and 6 hours. Tubulin protein was blotted as an internal control.

(g) Representative image of EYFP-IMA1 signal intensity profile in response to +Fe, +Fe with flg22, -Fe and -Fe with flg22 treatment in differentiation zone of roots in *pIMA1::EYFP-IMA1;ima8x* and *pIMA1::EYFP-IMA1;btsl1,2*. The white line in YFP channel indicates the line for signal quantification. The red dashed lines indicate the boundary between the ground tissue and the stele. Scale bar, 50 μm.

(h-j) Quantification of Normalized total IMA1 signal intensity (h), Normalized IMA1 signal intensity in epidermis and cortex (i) and IMA1 signal diameter (j) in differentiation zone of roots in *pIMA1::EYFP-IMA1;ima8x* and *pIMA1::EYFP-IMA1;btsl1,2*. The seedlings were pre-treated with +Fe/-Fe 36 hours with/without flg22 and treated with 100 μM CHX for 2 hours before imaging. Different letters indicate statistically significant differences between different conditions analyzed by one-way ANOVA and Fisher's LSD test($p<0.05$).

(k) Schematic of flg22-mediated IMA1 depletion in the outer cell layers (epidermis, cortex, and endodermis) and IRT1 repression in epidermis in response to +Fe, -Fe and -Fe with flg22 treatment respectively. By contrast, IMA1 is not fully degraded in *btsl1,2* in the outer cell layers upon flg22 treatment, resulting in IRT1 level maintenance in epidermis.

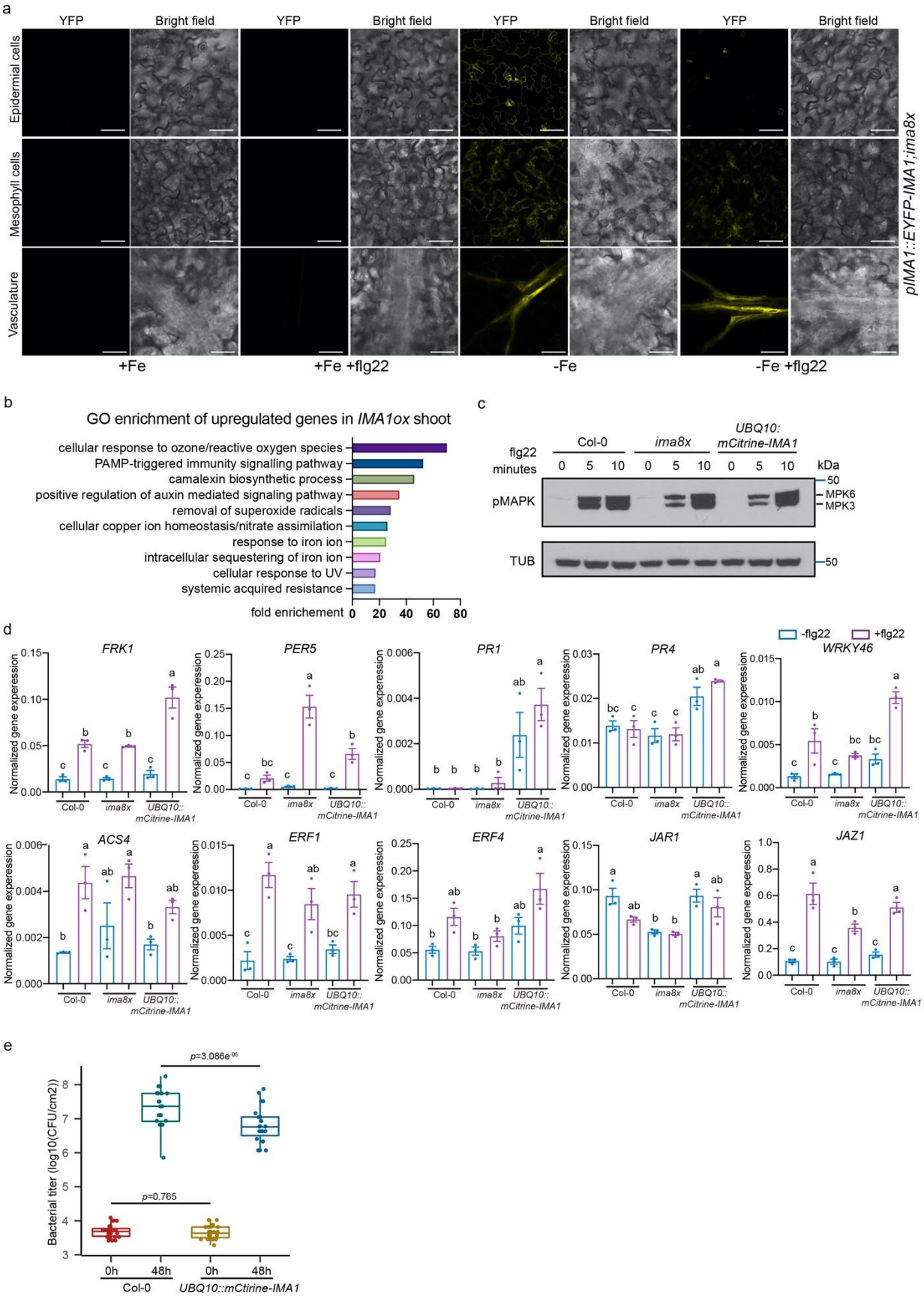
a
YFP
Bright field
Epidermial cells
Mesophyll cells
Vasculature
pIMA1::EYFP-IMA1;ima8x
+Fe
+Fe +flg22
-Fe
-Fe +flg22
b
GO enrichment of upregulated genes in IMA1ox shoot
cellular response to ozone/reactive oxygen species
PAMP-triggered immunity signalling pathway
camalexin biosynthetic process
positive regulation of auxin mediated signaling pathway
removal of superoxide radicals
cellular copper ion homeostasis/nitrate assimilation
response to iron ion
intracellular sequestering of iron ion
cellular response to UV
systemic acquired resistance
fold enrichement 0 20 40 60 80
c
flg22
minutes
Col-0
ima8x
UBQ10: mCitrine-IMA1
0 5 10 0 5 10 0 5 10
kDa
pMAPK
MPK6
MPK3
TUB
50
d
-flg22
+flg22
FRK1
PER5
PR1
PR4
WRKY46
ACS4
ERF1
ERF4
JAR1
JAZ1
Normalized gene expression
Col-0
ima8x
UBQ10:: mCitrine-IMA1
e
p=3.086e-05
p=0.765
Bacterial titer (log10(CFU/cm2))
0h
48h
Col-0
UBQ10::mCtirine-IMA1

1121

Extended Data figure 9. IMA1 mediates defense responses to different pathogens in the shoot.
(a) Confocal images of *pIMA1::EYFP-IMA1;ima8x* responses to +Fe, +Fe with flg22, -Fe and -Fe with flg22 in the shoot. Three different zones were imaged: Epidermal cells, Mesophyll cells and Vasculature. The cytosolic and nuclear localized EYFP-IMA1 signals (yellow channel) are visualized with bright field (bright field channel). For each treatment, a representative single confocal section is shown. Scale bar, 50 µm
(b) Gene ontology analysis of upregulated genes in *IMA1ox* compared with Col-0 in the shoot. GO term analysis is performed by using PANTHER17.0 (p-value<0.05). X axis, fold enrichment.
(c) Western blots showing MAPK phosphorylation by flg22 in Col-0, *ima8x* and *UBQ10::mCitrine-IMA1* shoot in response to flg22. The shoot parts were treated with 1µM flg22 for 0, 5 and 10 minutes. Tubulin protein was blotted as an internal control.
(d) Gene expression analysis in response to +Fe and +Fe with flg22 by quantitative RT-PCR. The gene expression level is normalized to *ACT2* internal control. The shoot parts were treated with 1µM flg22 for 1 hour. The bar chart centers show means of 3 biological replicates and error bars show s.e.m. Different letters indicate statistically significant differences between different conditions analyzed by one-way ANOVA and Tukey's test ($p<0.05$).
(e) Growth of *Pseudomonas syringae* pv. *tomato* DC3000 in the leaves of Col-0 and *UBQ10::mCitrine-IMA1*. Bacteria were syringe-infiltrated at OD_{600}=0.001, and bacterial colony forming units (CFUs) were counted 0 and 48 hours after inoculation (hpi). n=22-24 biological replicates from three independent experiments. Different letters indicate statistically significant differences (adjusted $P < 0.01$; two-tailed Student's t-test followed by Benjamini–Hochberg method). Results are shown as box plots with boxes displaying the 25th–75th percentiles, the center line indicating the median and whiskers extending to the minimum and maximum values no further than 1.5× interquartile range.

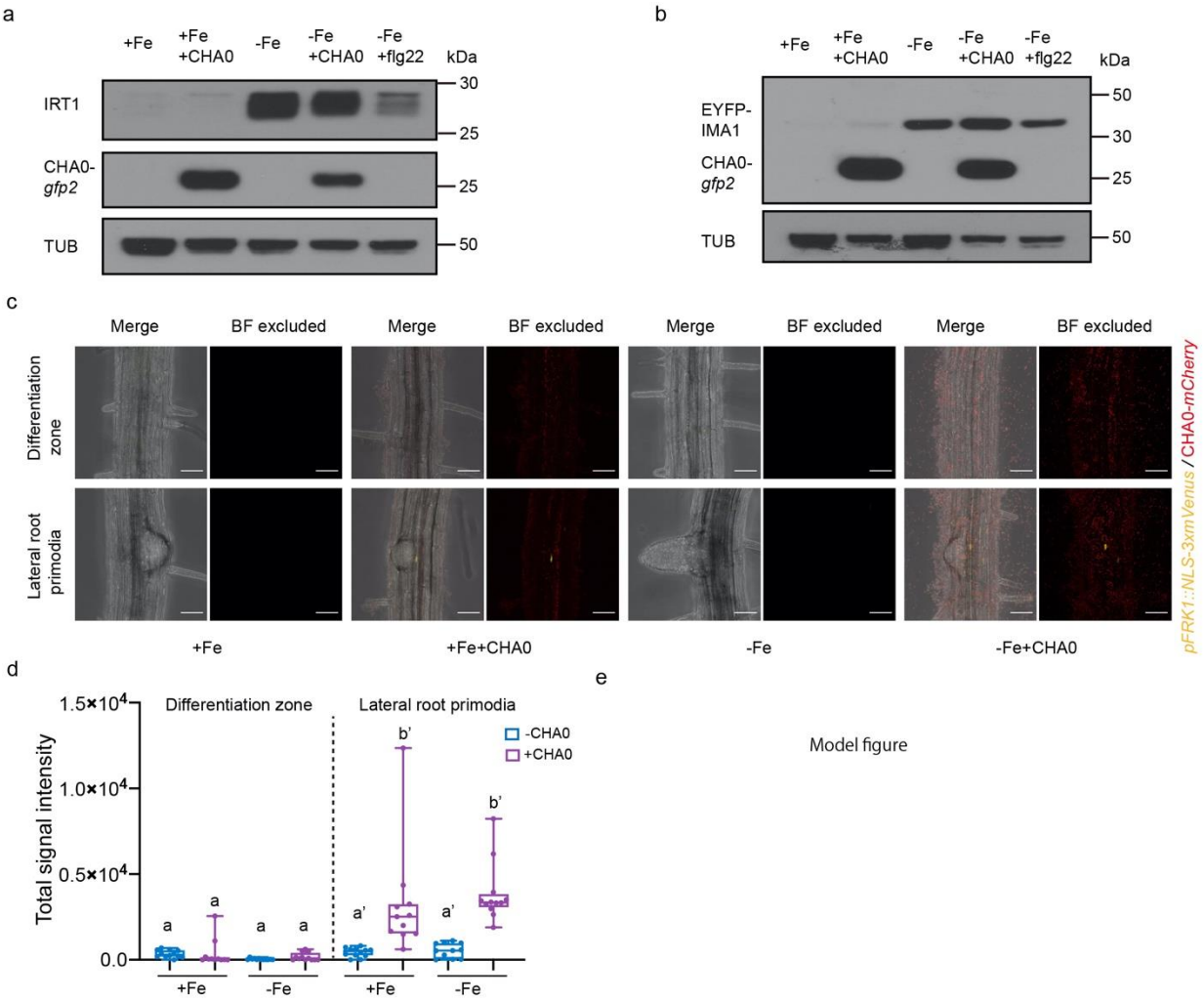

Extended Data figure 10. IRT1 and IMA1 accumulation is distinctly regulated by CHA0 or flg22 peptide.

(a) Western blots showing IRT1 protein levels in Col-0 roots in response to +Fe, +Fe+CHA0, -Fe, -Fe+CHA0 and -Fe+flg22 treatments. The inoculation of CHA0-*gfp2* was detected by anti-GFP western blot. Tubulin protein was blotted as an internal control.
(b) Western blots showing IMA1 protein levels in *pIMA1::EYFP-IMA1;ima8x* roots in response to +Fe, +Fe+CHA0, -Fe, -Fe+CHA0 and -Fe+flg22 treatment. The EYFP-IMA1 and the inoculation of CHA0-*gfp2* were detected by anti-GFP western blot. Tubulin protein was blotted as an internal control.
(c) The promoter activity of *FRK1* of *pFRK1::NLS-3xmVenus* responses to +Fe, +Fe+CHA0, -Fe, -Fe+CHA0 in differentiation zone or at lateral root primordia. Scale bar, 50 μm.
(d) Quantification of the total signal intensity of the promoter activity of *FRK1* in response to +Fe, +Fe+CHA0, -Fe, -Fe+CHA0 in differentiation zone or at lateral root primordia. Different letters indicate statistically significant differences between different conditions analyzed by one-way ANOVA and Fisher's LSD test($p<0.05$).
(e) Working model

REFERENCES

1 Hentze, M. W., Muckenthaler, M. U., Galy, B. & Camaschella, C. Two to tango: regulation of Mammalian iron metabolism. *Cell* **142**, 24-38, doi:10.1016/j.cell.2010.06.028 (2010).

2 Brown, J. C. Iron chlorosis in plants. *Advances in Agronomy* **13**, 329-369 (1961).

3 Yilmaz, B. & Li, H. Gut Microbiota and Iron: The Crucial Actors in Health and Disease. *Pharmaceuticals (Basel)* **11**, doi:10.3390/ph11040098 (2018).

4 Seyoum, Y., Baye, K. & Humblot, C. Iron homeostasis in host and gut bacteria - a complex interrelationship. *Gut Microbes* **13**, 1-19, doi:10.1080/19490976.2021.1874855 (2021).

5 Ganz, T. & Nemeth, E. Iron homeostasis in host defence and inflammation. *Nature Reviews Immunology* **15**, 500-510, doi:10.1038/nri3863 (2015).

6 Harbort, C. J. *et al.* Root-Secreted Coumarins and the Microbiota Interact to Improve Iron Nutrition in Arabidopsis. *Cell Host Microbe* **28**, 825-837 e826, doi:10.1016/j.chom.2020.09.006 (2020).

7 Stringlis, I. A. *et al.* MYB72-dependent coumarin exudation shapes root microbiome assembly to promote plant health. *Proceedings of the National Academy of Sciences of the United States of America* **115**, E5213-e5222, doi:10.1073/pnas.1722335115 (2018).

8 Romera, F. J. *et al.* Induced Systemic Resistance (ISR) and Fe Deficiency Responses in Dicot Plants. *Front Plant Sci* **10**, 287, doi:10.3389/fpls.2019.00287 (2019).

9 Zamioudis, C. *et al.* Rhizobacterial volatiles and photosynthesis-related signals coordinate MYB72 expression in Arabidopsis roots during onset of induced systemic resistance and iron-deficiency responses. *Plant J* **84**, 309-322, doi:10.1111/tpj.12995 (2015).

10 Aznar, A., Patrit, O., Berger, A. & Dellagi, A. Alterations of iron distribution in Arabidopsis tissues infected by Dickeya dadantii. *Molecular Plant Pathology* **16**, 521-528, doi:https://doi.org/10.1111/mpp.12208 (2015).

11 Xing, Y. *et al.* Bacterial effector targeting of a plant iron sensor facilitates iron acquisition and pathogen colonization. *Plant Cell* **33**, 2015-2031, doi:10.1093/plcell/koab075 (2021).

12 Nobori, T. *et al.* Transcriptome landscape of a bacterial pathogen under plant immunity. *Proceedings of the National Academy of Sciences of the United States of America* **115**, E3055-e3064, doi:10.1073/pnas.1800529115 (2018).

13 Gu, S. *et al.* Competition for iron drives phytopathogen control by natural rhizosphere microbiomes. *Nat Microbiol* **5**, 1002-1010, doi:10.1038/s41564-020-0719-8 (2020).

14 Meziane, H., I, V. D. S., LC, V. A. N. L., Höfte, M. & Bakker, P. A. Determinants of Pseudomonas putida WCS358 involved in inducing systemic resistance in plants. *Mol Plant Pathol* **6**, 177-185, doi:10.1111/j.1364-3703.2005.00276.x (2005).

15 Verbon, E. H. *et al.* Iron and Immunity. *Annual Review of Phytopathology* **55**, 355-375, doi:10.1146/annurev-phyto-080516-035537 (2017).

16 Platre, M. P. *et al.* The receptor kinase SRF3 coordinates iron-level and flagellin dependent defense and growth responses in plants. *Nature Communications* **13**, 4445, doi:10.1038/s41467-022-32167-6 (2022).

17 Colangelo, E. P. & Guerinot, M. L. The essential basic helix-loop-helix protein FIT1 is required for the iron deficiency response. *Plant Cell* **16**, 3400-3412, doi:10.1105/tpc.104.024315 (2004).
18 Grillet, L., Lan, P., Li, W., Mokkapati, G. & Schmidt, W. IRON MAN is a ubiquitous family of peptides that control iron transport in plants. *Nature plants* **4**, 953-963, doi:10.1038/s41477-018-0266-y (2018).
19 Kroh, G. E. & Pilon, M. Connecting the negatives and positives of plant iron homeostasis. *New Phytologist* **223**, 1052-1055, doi:https://doi.org/10.1111/nph.15933 (2019).
20 Ngou, B. P. M., Ahn, H.-K., Ding, P. & Jones, J. D. G. Mutual potentiation of plant immunity by cell-surface and intracellular receptors. *Nature* **592**, 110-115, doi:10.1038/s41586-021-03315-7 (2021).
21 Yuan, M. *et al.* Pattern-recognition receptors are required for NLR-mediated plant immunity. *Nature* **592**, 105-109, doi:10.1038/s41586-021-03316-6 (2021).
22 Faulkner, C. *et al.* LYM2-dependent chitin perception limits molecular flux via plasmodesmata. *Proceedings of the National Academy of Sciences of the United States of America* **110**, 9166-9170, doi:10.1073/pnas.1203458110 (2013).
23 Vatén, A. *et al.* Callose biosynthesis regulates symplastic trafficking during root development. *Dev Cell* **21**, 1144-1155, doi:10.1016/j.devcel.2011.10.006 (2011).
24 Li, Y. *et al.* IRON MAN interacts with BRUTUS to maintain iron homeostasis in Arabidopsis. *Proceedings of the National Academy of Sciences* **118**, e2109063118, doi:doi:10.1073/pnas.2109063118 (2021).
25 Rodríguez-Celma, J. *et al.* Arabidopsis BRUTUS-LIKE E3 ligases negatively regulate iron uptake by targeting transcription factor FIT for recycling. *Proceedings of the National Academy of Sciences* **116**, 17584-17591, doi:doi:10.1073/pnas.1907971116 (2019).
26 Schmidt, W., Michalke, W. & Schikora, A. Proton pumping by tomato roots. Effect of Fe deficiency and hormones on the activity and distribution of plasma membrane H+-ATPase in rhizodermal cells. *Plant, Cell & Environment* **26**, 361-370, doi:https://doi.org/10.1046/j.1365-3040.2003.00967.x (2003).
27 Liu, L. *et al.* Extracellular pH sensing by plant cell-surface peptide-receptor complexes. *Cell* **185**, 3341-3355.e3313, doi:https://doi.org/10.1016/j.cell.2022.07.012 (2022).
28 Yu, K. *et al.* Rhizosphere-Associated Pseudomonas Suppress Local Root Immune Responses by Gluconic Acid-Mediated Lowering of Environmental pH. *Current Biology* **29**, 3913-3920.e3914, doi:https://doi.org/10.1016/j.cub.2019.09.015 (2019).
29 Liu, Y. *et al.* Plant commensal type VII secretion system causes iron leakage from roots to promote colonization. *Nature Microbiology*, doi:10.1038/s41564-023-01402-1 (2023).
30 Verbon, E. H. *et al.* Rhizobacteria-Mediated Activation of the Fe Deficiency Response in Arabidopsis Roots: Impact on Fe Status and Signaling. *Frontiers in Plant Science* **10**, doi:10.3389/fpls.2019.00909 (2019).
31 Zhou, F. *et al.* Co-incidence of Damage and Microbial Patterns Controls Localized Immune Responses in Roots. *Cell* **180**, 440-453.e418, doi:10.1016/j.cell.2020.01.013 (2020).
32 Sanchez, K. K. *et al.* Cooperative Metabolic Adaptations in the Host Can Favor Asymptomatic Infection and Select for Attenuated Virulence in an Enteric Pathogen. *Cell* **175**, 146-158.e115, doi:10.1016/j.cell.2018.07.016 (2018).

33 Hiruma, K. *et al.* Root Endophyte Colletotrichum tofieldiae Confers Plant Fitness Benefits that Are Phosphate Status Dependent. *Cell* **165**, 464-474, doi:10.1016/j.cell.2016.02.028 (2016).
34 Castrillo, G. *et al.* Root microbiota drive direct integration of phosphate stress and immunity. *Nature* **543**, 513-518, doi:10.1038/nature21417 (2017).
35 Gruber, B. D., Giehl, R. F. H., Friedel, S. & von Wirén, N. Plasticity of the Arabidopsis Root System under Nutrient Deficiencies *Plant Physiology* **163**, 161-179, doi:10.1104/pp.113.218453 (2013).
36 Wyrsch, I., Domínguez-Ferreras, A., Geldner, N. & Boller, T. Tissue-specific FLAGELLIN-SENSING 2 (FLS2) expression in roots restores immune responses in Arabidopsis fls2 mutants. *New Phytologist* **206**, 774-784, doi:https://doi.org/10.1111/nph.13280 (2015).
37 Cao, M. *et al.* TMK1-mediated auxin signalling regulates differential growth of the apical hook. *Nature* **568**, 240-243, doi:10.1038/s41586-019-1069-7 (2019).
38 Gautam, C. K., Tsai, H.-H. & Schmidt, W. A Quick Method to Quantify Iron in Arabidopsis Seedlings. *Bio-protocol* **12**, e4342, doi:10.21769/BioProtoc.4342 (2022).
39 Bayle, V., Platre, M. P. & Jaillais, Y. Automatic Quantification of the Number of Intracellular Compartments in Arabidopsis thaliana Root Cells. *Bio-protocol* **7**, doi:10.21769/BioProtoc.2145 (2017).
40 Santi, S. & Schmidt, W. Dissecting iron deficiency-induced proton extrusion in Arabidopsis roots. *New Phytol* **183**, 1072-1084, doi:10.1111/j.1469-8137.2009.02908.x (2009).
41 Gujas, B., Alonso-Blanco, C. & Hardtke, C. S. Natural Arabidopsis brx loss-of-function alleles confer root adaptation to acidic soil. *Current biology : CB* **22**, 1962-1968, doi:10.1016/j.cub.2012.08.026 (2012).
42 Berardini, T. Z. *et al.* The Arabidopsis information resource: Making and mining the "gold standard" annotated reference plant genome. *Genesis* **53**, 474-485, doi:10.1002/dvg.22877 (2015).
43 Dobin, A. *et al.* STAR: ultrafast universal RNA-seq aligner. *Bioinformatics (Oxford, England)* **29**, 15-21, doi:10.1093/bioinformatics/bts635 (2012).
44 Robinson, M. D., McCarthy, D. J. & Smyth, G. K. edgeR: a Bioconductor package for differential expression analysis of digital gene expression data. *Bioinformatics (Oxford, England)* **26**, 139-140, doi:10.1093/bioinformatics/btp616 (2010).
45 Gu, Z., Eils, R. & Schlesner, M. Complex heatmaps reveal patterns and correlations in multidimensional genomic data. *Bioinformatics (Oxford, England)* **32**, 2847-2849, doi:10.1093/bioinformatics/btw313 (2016).